Grain Boundaries in Multicrystalline Silicon 19

Matthias Trempa, Georg Müller, Jochen Friedrich, and Christian Reimann

Contents

M. Trempa (✉)
Fraunhofer Institute for Integrated Systems and Device Technology (IISB), Erlangen, Germany
e-mail: matthias.trempa@iisb.fraunhofer.de

G. Müller
Crystal Consulting, Langensendelbach, Germany
e-mail: mueller@crystalconsulting.de

J. Friedrich · C. Reimann
Fraunhofer Technology Center Semiconductor Materials (THM), Freiberg, Germany

Fraunhofer Institute for Integrated Systems and Device Technology (IISB), Erlangen, Germany
e-mail: jochen.friedrich@iisb.fraunhofer.de; christian.reimann@iisb.fraunhofer.de

D. Yang (ed.), *Handbook of Photovoltaic Silicon*,
https://doi.org/10.1007/978-3-662-56472-1_25

Abstract

Directionally solidified (DS) silicon is typically multicrystalline (mc), i.e., it contains per definition grain boundaries. Even so-called quasi-mono silicon is not free of grain boundaries. The crystallographic arrangement of neighboring grains is used for a definition of the certain types of grain boundaries by the so-called coincidence site lattice parameter Σ. It turns out that the predominant types of grain boundaries are twin ($\Sigma = 3$), small angle ($\Sigma \sim 1$), and large angle ("random") grain boundaries. For the solar cell application, it is of great relevance that the nontwin boundaries are often accompanied by dislocation defects. These dislocations, especially their clusters, are well known to reduce the minority charge carrier lifetime and hence the efficiency of solar cells. Therefore, the corresponding characterization methods for the types of grain boundaries, their length, spatial distribution, and grain size will be presented in this chapter.

The main part of the chapter presents a detailed treatment of the occurrence of the various types of grain boundaries and the related dislocations structures for different variants of the DS method. The most important DS variants differ from each other mainly by the seeding and nucleation processes which result in different sizes of the grains and also different prevailing grain boundaries. The so-called classic mc, dendritic mc, and quasi-mono Si material have relatively large average grain sizes ranging from mm up to cm. The solar cell performance of this material is mainly limited by the occurrence of dislocation structures which can easily spread in the relatively large grains. This problem seems to be decreased in a recently developed fine grained material (micro-meter up to mm scale). The variety of nucleation concepts to achieve a fine grained structure reaches from seeding with small Si feed or non-Si particles to specially structured profiles of the crucible bottom. The resulting higher performance of solar cells is promising for the future and gave reason to call the material high performance mc Si (HPM).

The whole chapter includes results of recent worldwide research and development activities but provides also its proving under production-like conditions. All results are illustrated by corresponding figures and allocated to important references.

Keywords

Multicrystalline silicon · Grain boundaries · Directional solidification · Small angle grain boundaries · Large angle grain boundaries · Twin boundaries · Random grain boundaries · Laue scanner method

Introduction

Most solar cells are produced by using either monocrystalline silicon grown by the Czochralski (CZ) crystal pulling method (▶ Chap. 6, "Growth of Crystalline Silicon for Solar Cells: Czochralski Si") or multicrystalline silicon obtained by directional solidification (DS) of the melt in a crucible (▶ Chap. 7, "Growth of Multicrystalline

Silicon for Solar Cells: The High-Performance Casting Method"). The DS equipment and process technology is less expensive compared to Czochralski. However, solar cells made from DS silicon have about 2% less efficiency compared to CZ-based cells. The main reason for this difference is the fact that DS silicon is not mono- but multicrystalline which means it contains defects like grain boundaries and dislocations, whereas CZ silicon is free of grain boundaries (= definition of monocrystalline) and typically free of dislocations. In combination with a higher amount of metals in DS silicon, the crystallographic defects like grain boundaries get even more detrimental to the solar cell performance.

Grain boundaries are by definition crystal regions where two grains i.e., monocrystalline silicon regions of different crystallographic orientation are neighboring each other. It is obvious that in between the two grains a transition region exists were the atoms are shifted in general from their regular positions in comparison to the lattice of a perfect monocrystal. For example, dislocation defects are typically occurring within the boundary region. It will be shown that the specific difference in orientation between the two grains has an important influence on the degree of lattice disorder within the grain boundary. That means the effect of a grain boundary on the electronic material properties and hence on the solar cell performance can considerably differ depending on the "type of grain boundary."

For example, certain types of grain boundaries can reduce the formation, movement, or multiplication of dislocations which are accompanying the grain boundary defects. Furthermore, certain grain boundaries can interfere with gettering mechanisms during solar cell fabrication processes like the phosphorus or hydrogen gettering.

With respect to the future development of silicon-based solar cells, it is important to consider which potential the DS process has regarding a further improvement of the material quality, i.e., reduction of deleterious crystal defects like grain boundaries and accompanying dislocations. From the point of view of research and development of silicon material preparation, one can state that the work on the CZ crystal growth process started already around 1950. It was mainly driven in the past by the requirements of micro- and power electronic devices. The DS process of silicon was from the beginning only of interest for photovoltaic applications. Intensive research and development activities on DS of silicon started fairly later between 2000 and 2010. Therefore, one can expect that there still exists a considerable potential to improve the DS process further by future research and development activities, especially with respect to an optimization of grain boundary growth.

It is the main goal of this chapter to show how certain conditions and parameters of the DS process like seeding, crucible preparation, or thermal profiles are related to the formation of certain types of grain boundaries (section "Formation of grain boundaries during directional solidification (DS)"). Based on these results, one can draw certain conclusions for "grain boundary engineering," i.e., optimizing the DS process to achieve high solar cell performance material. In the first part, the criteria for classifying the various types of grain boundaries will be introduced and its specific influences on the solar cell performance. In the following an overview of characterization methods for grain boundary types is given with special emphasis on methods which are applicable to the complete solar wafer area of 156×156 mm^2.

Grain Boundaries and Their Influences on Solar Cell Performance

Classification and Types of Grain Boundaries

In the previous chapters of this handbook, e.g., ▶ Chaps. 17, "Metal Impurities and Gettering in Crystalline Silicon" or ▶ 18, "Defects in Crystalline Silicon: Dislocations," it has been shown that various types of crystal defects can occur in photovoltaic Si depending on the production method of the Si crystals or ingots. This chapter treats grain boundaries which are occurring only in multicrystalline Si obtained typically by directional solidification and "kerfless processes" including ribbon growth and direct deposition on alternative substrates.

By definition, "multi"-crystalline (mc) Si consists of a number of monocrystalline grains which are separated from each other by a grain boundary. Typically, the grains in a multicrystalline material like Si have different crystallographic orientations as shown, for example, in Fig. 1 (where the different grain orientations are visible due to the different light reflection).

That means a grain boundary is a transition region between two monocrystalline crystal regions where the regular crystal lattice is distorted.

This misfit on the atomistic scale of a grain boundary is the reason why grain boundaries must be considered generally as a crystal defect which can have deleterious influences on the electronic properties of the solar cell material. However, it is also obvious that the defect generating degree of misfit in a certain grain boundary depends on the orientation of the adjacent crystal lattices of the two neighboring grains. Therefore, one should expect a different degree of deleterious influence on the solar cell performance depending on the orientation between the two grains. In fact the first goal of this chapter will be to explain and demonstrate which type of

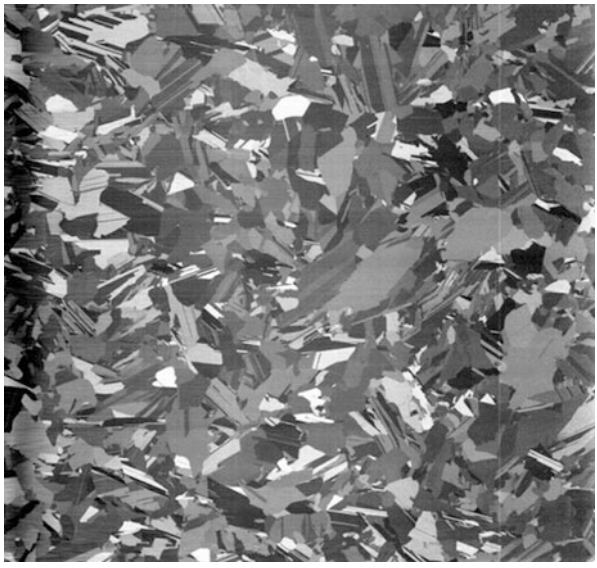

Fig. 1 Typical mc-wafer (156×156 mm^2) after structural etching (details see later). (© Fraunhofer IISB)

grain boundary in mc-Si is less deleterious and can be tolerated in solar cells and which one is more harmful and should be avoided.

Description and Types of Grain Boundaries

A grain boundary can be fully described by five independent macroscopic degrees of freedom (DOFs). Three DOFs specify the mutual misorientation of the two grains and two more DOFs are needed to define the orientation of the grain boundary itself between the misorientated grains. Considering the necessity of five DOFs for a complete crystallographic description of a grain boundary, one can expect a huge number of different grain boundaries. However, it turns out that materials like Si prefer only a few types of grain boundaries for energetic reasons. Therefore, it is reasonable to categorize the grain boundaries into groups according to the relationship among individual DOFs.

A very special grain boundary occurring relatively often in mc-Si is the so-called "small angle grain boundary" (SAGB) in contrast to all other grain boundaries which are named as large angle grain boundaries. In SAGBs, the angle of misorientation between the two adjacent grains is small (a few degrees or less). In this case, the lattice mismatch on the atomic scale can be described by an array of edge-type dislocations along the grain boundary. This model is illustrated in Fig. 2 for a cubic primitive lattice. The angle θ of the misorientation between the two lattices can be related to the Burgers vector b and the distance D between two dislocations.

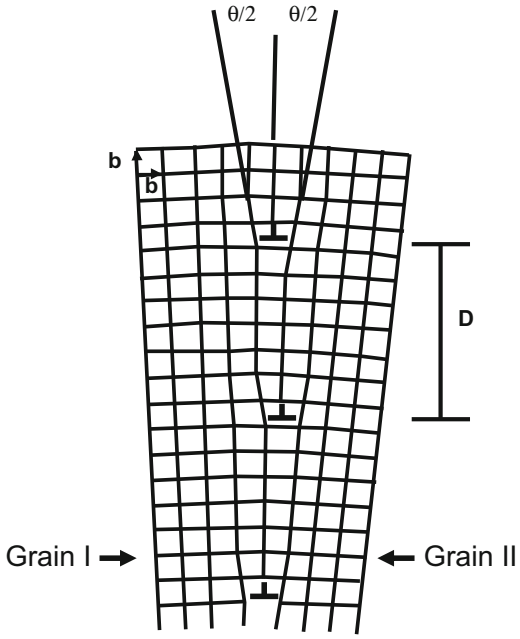

Fig. 2 Sketch of a small-angle grain boundary: Two grains (I and II) having a common [001] axis and angular difference in orientation of θ are forming a low-angle grain boundary which can be considered to consist of an array of edge dislocations

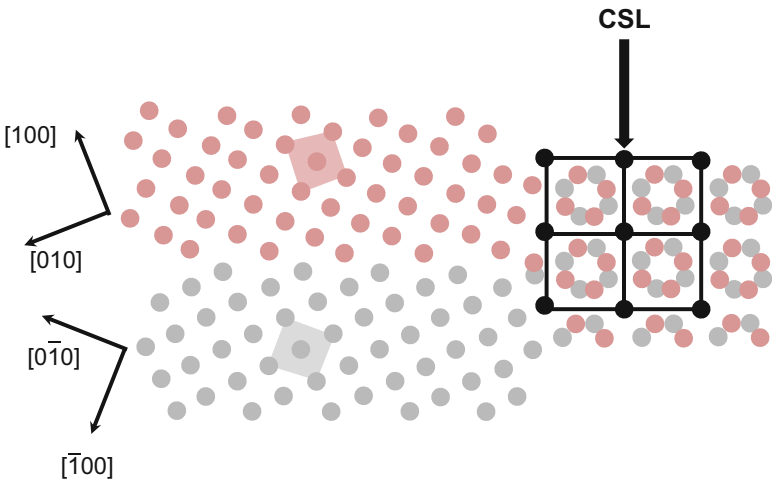

Fig. 3 Sketch for an evaluation of the coincidence site lattice (CSL). See also text

$$D = \frac{b}{2\sin\left(\frac{\theta}{2}\right)} \approx \frac{b}{\theta}$$

For very small angles θ, the relation can be approximated by $D = b/\theta$. This relation allows for an estimation of the tilt angle between the grains if the dislocation density in the grain boundary is known. For increasing grain boundary angle θ, the spacing D between the dislocations decreases and the model above becomes no longer useful. The common concept for these cases is the coincidence site lattice (CSL) model. It is based on the fact that for certain orientations of the two lattices of the two neighboring grains, parts of the lattice sites coincide if one continues the two lattices into the respective grains. This construction is exemplified by Fig. 3.

The CSL model is very popular because it allows describing the grain boundary by only one parameter Σ instead of five. Σ is defined by the ratio between the number of lattice sites within the unit cell of the coincidence lattice and the unit cell of the crystal, i.e., Si. This ratio is equal to the volume of the unit cell of the coincidence lattice divided by the volume of the Si unit cell. According to this definition, the values of Σ are always odd numbers. Σ equal to one defines the monocrystal. The small angle grain boundary discussed above would have a Σ value which is close to one. The lowest integer Σ value except one is $\Sigma = 3$ which describes a so-called first order twin boundary. Twin boundaries are grain boundaries with the highest symmetry and lowest disturbance of the crystal lattice. Figure 4 shows a typical $\Sigma = 3$ twin configuration of Si where the two Si grains have the same <111>-orientation.

Within the twin grain boundary, all Si bonds are saturated, i.e., no open dangling bonds exist. The lattices of the two grains are twisted by 60° to each other within the twin plane only. The formation energy of this grain boundary is very low because it

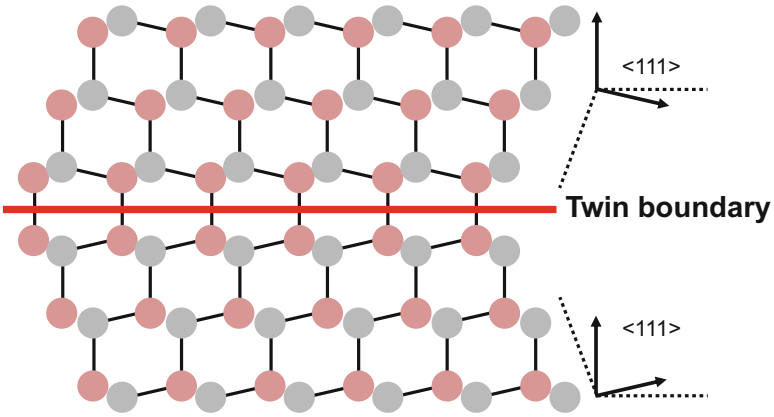

Fig. 4 Sketch of a <111> Σ = 3 twin boundary

corresponds just to one stacking fault within the sequence of the Si layers. The energy E_{SF} of the stacking fault formation in Si is relatively low ($E_{SF} = 26$ mJ/m^2). Therefore, its formation can occur very often during the growth of mc-Si.

Other types of twin boundaries have values of $\Sigma = \Sigma 3^n$ whereas their occurrence in mc-Si material decreases in frequency with increasing Σ value from Σ3 to Σ9 to Σ27. Also other Σ grain boundaries like Σ5 or Σ11 exist but very rarely. In theory, very large Σ values can be calculated; however, a grain boundary with $\Sigma > 27$ is practically stated as a random large angle grain boundary due to its low symmetry. It has to be noted that one Σ type can be formed by several lattice operations meaning the rotation about a specific crystallographic axis by certain degrees. For instance, there exists beside the already mentioned Σ3 {111} (rotation angle: 60°) also a Σ3 {112} grain boundary (rotation angle 180°). Further details, for example, on orientation relations between grains of certain Σ types are discussed in literature (see Vlachavas 1985; Wilhelm 1971).

For a general application of the CSL concept including large angle grain boundaries, one has to consider that in a real crystal, certain deviations of the atoms from the exact CSL relationship may exist. Therefore, it is important to define a criterion for the permissible deviation from exact coincidence. Such a criterion was given by Brandon (1966). Its derivation is based on the assumption that deviations from the exact lattice site coincidence can be attributed to slight orientation deviations caused by arrays of dislocations. Such a dislocation model was already used above for the description of small angle grain boundaries (compare Fig. 2). Brandon's criterion gives a relation for the maximum permissible deviation angle θ in dependence of the CSL parameter Σ

$$\theta = \theta_o \, (\Sigma)^{-1/2}$$

where θ_o is constant about 15°. According to this criterion, the transition from a small angle grain boundary ($\Sigma \sim 1$) to a large angle grain boundary is at $\theta \sim 15^\circ$.

Properties of Grain Boundaries

Energy of Grain Boundaries

Each grain boundary means an extra energy in the crystal lattice compared to the single crystal. This extra energy (grain boundary energy) has the unit J/m^2 and is specific for each type of grain boundary. In Fig. 5, the specific grain boundary energy for Si is plotted versus the tilt angle θ against the [110] plane. Certain Σ-values have minima of the grain boundary energy especially the Σ3 – {111} twin boundary – with a tilt angle of about 70° to the [110] direction. These energetic minima correlate with the observation that twin boundaries, especially the type Σ3, have the highest frequency of occurrence compared to other types of grain boundaries. Obviously, the growing mc crystal follows the thermodynamic principle of minimizing its Gibbs free energy.

It explains also the observation that grain boundaries with lower symmetry split into grain boundaries with higher symmetry, for example, R → Σ3 + Σ27 (see Fig. 6 on the left). Another often observed phenomenon is the split of low energy grain boundaries from nonperfect Σ grain boundaries or grain boundaries with higher energy, e.g., R → R* + Σ3 (see Fig. 6 on the right). In these cases, the gain in grain boundary energy is obviously larger than the extra energy for the extension of the grain boundary length.

Decoration of Grain Boundaries with Impurity Atoms

The Gibbs free energy of a grain boundary can also be reduced by incorporation of foreign atoms, i.e., impurity atoms. This process is driven by thermodynamics but controlled by kinetics. The diffusive transport of the impurity atoms from the interior

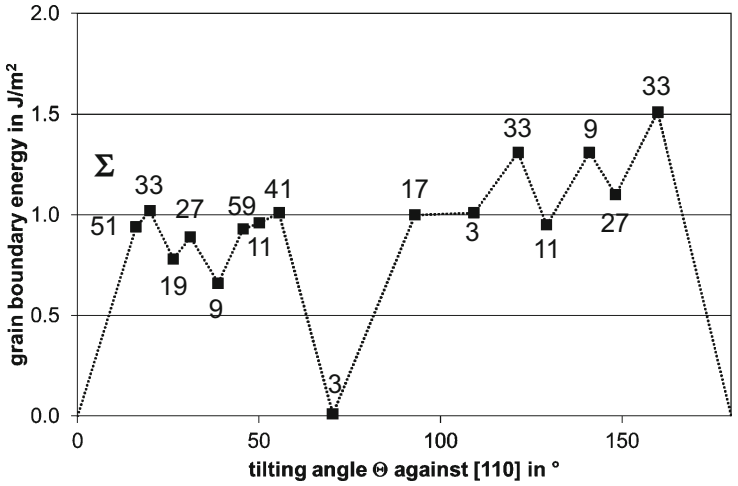

Fig. 5 Grain boundary energy in Si in dependence on tilting angle θ against [110] direction. The corresponding values of Σ are given at the top. θ = 0° and θ = 180° correspond to Σ = 1. Values after Kohyama et al. (1986)

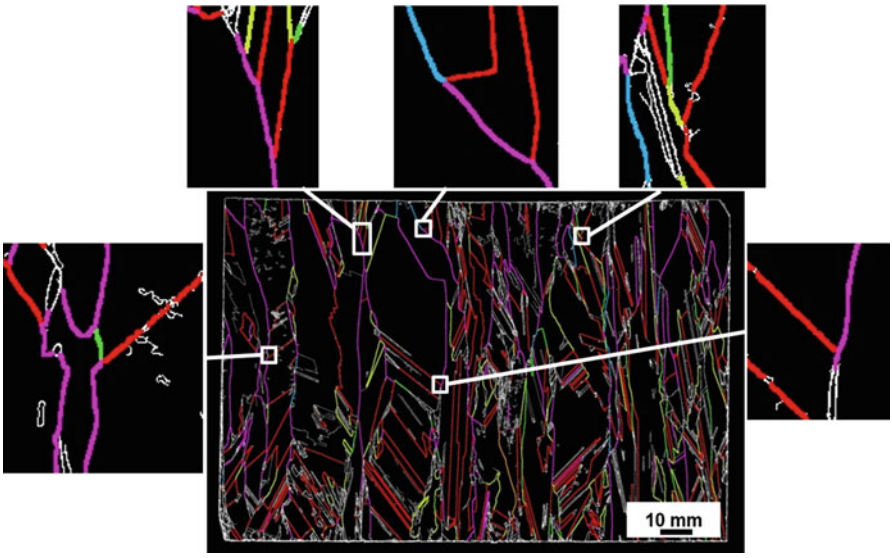

Fig. 6 Splitting of low symmetry grain boundaries into high symmetry grain boundaries during growth of mc Si, measured on a cut parallel to the growth direction. The colors represent the different grain boundary types; Σ3 (red), Σ9 (yellow), Σ27 (green), and R (purple). (© Fraunhofer IISB)

of a grain into the grain boundary depends on the diffusivity and the temperature – time conditions. It can be expressed in terms of a diffusion length. As a consequence, the region within the diffusion length around a grain boundary is denuded from impurity atoms which are collected within the grain boundary. The latter effect is called "gettering" and can lead to an increased minority charge carrier lifetime τ (see, e.g., Martinuzzi et al. 2007). Additionally, the diffusion velocity of impurity atoms is increased along grain boundaries. This can be observed in typical lifetime images of mc Si bricks or wafers (see Fig. 7 on the right) where metal atoms diffuse from the highly contaminated bottom and top into the ingot volume and cause local areas of lower lifetime at grain boundaries and dislocation clusters.

The minority charge carrier lifetime τ is one of the main material parameters, which determines the solar cell performance and is often directly correlated to the concentration of the impurity (mainly metal) atoms (▶ Chap. 17, "Metal Impurities and Gettering in Crystalline Silicon"). A direct clear evidence of the impurity accumulation in grain boundaries of mc-Si was given by Buonassisi et al. (2007) and is shown in Fig. 7.

This result shows additionally that the metal content of grain boundaries increases with increasing CSL number Σ. However, it has to be kept in mind that the accumulation of specific metal atoms in grain boundaries is depending on the specific diffusivity of the metal in Si. This effect was studied for various contaminating metals (Cu, Fe, Ni, Ti) (Buonassisi et al. 2007). They found a clear anticorrelation between the diffusivity and the fraction of impurities inside the grain which do not reach the grain boundary. Additionally it was shown (Bauer et al. 2007) that during the movement of the solid-liquid interface during the crystal growth process, carbon and nitrogen atoms

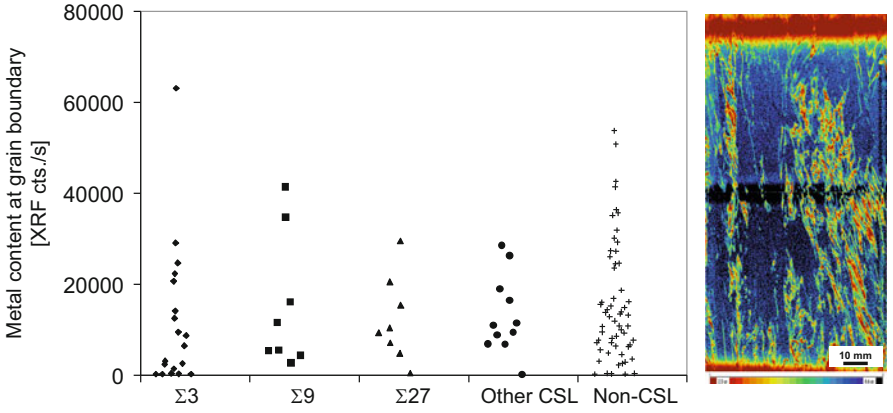

Fig. 7 Left: Accumulation of metal atoms at grain boundaries detected by X-ray fluorescence analysis for various types of grain boundaries. After Buonassisi et al. (2007). (Right) Lifetime image of a vertical section of an industrial mc Si brick from bottom (below) to top end. (© Fraunhofer IISB)

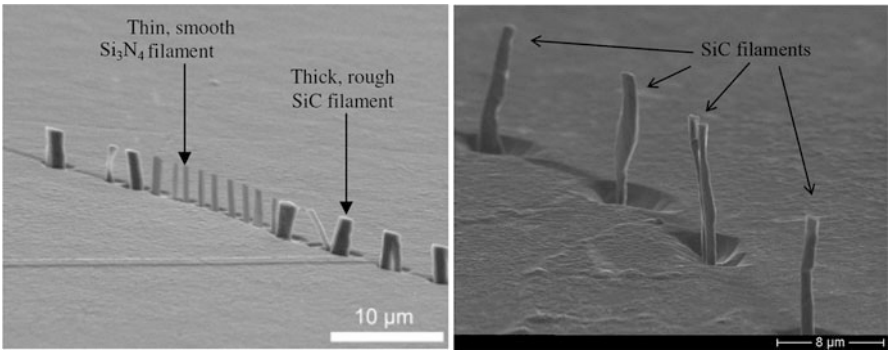

Fig. 8 SEM images of Si_3N_4 and SiC filaments along grain boundaries in mc silicon. After Bauer et al. (2007)

can be enriched in grain boundary grooves and lead to the formation of SiC and Si_3N_4 filaments along the grain boundary (compare Fig. 8).

Impact of Grain Boundaries on Electronic Properties

The most important impact of grain boundaries on solar cell performance is via its influence on the lifetime τ of the minority charge carriers. This effect is related to the classical Shockley-Hall-Read recombination mechanism of dangling bonds which are occurring at certain types of grain boundaries, dislocations, and metallic impurities accumulated within grain boundaries. The influence of grain boundaries on τ depends on their type and decoration by metallic impurities. Contaminated grain boundaries are decreasing τ mainly because of the metal impurities which form deep recombination levels in the Si band gap. Such contamination-related problems including electric short cuts by decorated grain boundaries can

generally be reduced by the corresponding purity of the Si feedstock (▶ Chap. 2, "Polysilicon and Its Characterization Methods") and proper purification measures during the DS process. "Pure," i.e., noncontaminated grain boundaries are considered to be less or even not harmful for τ. This holds at least for low Σ type grain boundaries, compare (Tsurekawa et al. 2007). Other grain boundary types may have also an influence on the mobility of the charge carriers, e.g., by scattering due to the potential barriers.

Dislocations and Grain Boundaries

Crystal defects in the form of dislocations are of enormous importance for the performance of Si solar cells (▶ Chap. 18, "Defects in Crystalline Silicon: Dislocations") Dislocations are mainly generated at grain boundaries during the solidification at the solid-liquid interface and can only be avoided reliably by growing a single crystal. That means the formation of grain boundaries in mc-Si is inherently connected with the formation and existence of dislocations. It was already shown in section "Classification and Types of Grain Boundaries" that small angle grain boundaries can be considered as an array of dislocations (compare Fig. 2). Also any deviations of grain boundaries from the ideal CSL criterion can be attributed to dislocations. Only perfect twin boundaries (means a deviation angle $\theta = 0$) like Σ3, Σ9, and Σ27 are free of dislocations. Therefore, it is not surprising that dislocations in mc-Si can be distributed very inhomogeneously according to the wide variety of different grain boundary types and especially due to the different orientations of glide planes in the neighboring grains in this material. Experimental results show that the density of dislocations and especially the formation of so-called dislocation clusters are strongly depending on the orientation of the grains with respect to the direction of solidification and to the orientation of neighboring grains. This can lead to a distribution where grains with a dislocation density of higher than 10^6 cm^{-2} are close to nearly dislocation-free grains.

In summary, one can state that one important prerequisite for producing high quality mc-Si based solar cells consists in a selection of such grain boundaries which do not provoke the formation and multiplication of dislocations within the grown Si ingot. Therefore, the nowadays typically used solidification processes for mc Si will be analyzed in detail with respect to the influence of the thermal boundary conditions and the seeding specifications on the formation of specific grain boundaries and the related dislocations (see section "Formation of Grain Boundaries During Directional Solidification (DS)"). Prior to that, the important methods of characterizing grain boundaries will be introduced.

Characterization of Grain Boundaries

Overview

Grain boundaries in Si can be characterized by a variety of methods. The selection of the proper method depends on the aim and the expenditure which can be made. A qualitative visualization of grains and grain boundaries is possible by viewing

the light which is reflected from a metallographically treated Si surface. This effect is due to the optical property of a crystalline Si surface that its reflectance is depending on the crystallographic orientation. Such pictures can be evaluated by image processing to provide data like the statistical distribution of the grain size or the total length of the grain boundaries. A quantitative evaluation of the crystallographic orientations of certain grains is possible by electron or X-ray diffraction methods. By combining the crystallographic orientation of various grains with their local position on a wafer, it is possible to display the grain boundaries according to their types, for example, in the CSL notation. This kind of characterization is very helpful for the optimization of solidification processes and will be used extensively in the section "Formation of grain boundaries during directional solidification (DS)".

So far the methods of characterization mentioned above relate mainly to the geometry and crystallographic orientation relations of grains and grain boundaries. Beyond that a variety of characterization tools is available which can be used to analyze material properties which are relevant for solar cells in relation to certain orientation and size of grains, types of grain boundaries, and their distribution. Among these methods are photoluminescence (PL), electron beam induced current (EBIC), X-ray diffraction, and electron microscopy (SEM, TEM). Table 1 gives an overview of the various characterization methods in relation to the objectives. More details are presented in the following sections.

Table 1 Characterization of grain boundaries

Objective	Method
Visualization of grains and grain boundaries	Optical microscopy after (chemo-) mechanical treatment & defect selective etching (also small angle grain boundaries and dislocations visible) Optical reflection analysis after metallographic treatment (only large angle grain boundaries visible)
Evaluation of grain size, distribution and total grain boundary length	Image processing of reflection images
Recording and determination of grain orientations on a sample surface ("orientation map")	Calibrated reflection image Electron back-scatter diffraction (EBSD) X-ray diffraction (Laue method)
Evaluation of types of grain boundaries and their local distribution	EBSD mapping (for small samples!) "Laue Scanner" (for full wafer size)
Evaluation of grain boundaries with a very high local resolution (down to atomic scale)	X-ray topography (XRT) Transmission electron microscopy (TEM)
Local evaluation of electronic properties in correlation with grain structure and grain boundaries	Photoluminescence (PL) Electron beam induced current (EBIC)

Optical Grain Detection and Analysis

The grain structure of a mc-Si sample or wafer, respectively, is already visible by the naked eye after sawing. This is due to the dependence of the reflectivity of visual light from the crystallographic orientation of a certain grain surface. The precision and information value of the optical grain detection can be improved by using a metallographic treatment (e.g., grinding, lapping) of the surface, an accompanied wafer texturing step and/or image processing. A state of the art in-line grain structure inspection requires fast measuring times and is therefore mostly limited to reflection measurements on as-sawn or textured wafers.

To visualize in detail crystallographic features like small and large angle grain boundaries as well as single dislocations (so-called etch pits), a number of etching solutions is reported in literature with different etching behavior (e.g., nonisotropic or isotropic). A selection of etchants is compiled in Table 2 together with their recipes and the applicability for different electrical resistivity ranges and grain orientations.

Table 2 Si etchants for grain boundary analysis after Sirtl and Adler (1961), Secco D'Aragona (1972), Wright-Jenkins (1977), Schimmel (1979), Yang (1984), and Sopori (1984)

Etchant	Typical etch rate (μm/min)	Resistivity range (Ωcm)	Remarks
Sirtl 1 HF (49%) 1 CrO_3 (5 M)	3.0 on (111)	Not specified	Not as good for (100) orientation
Secco 1 HF (49%) 1 $K_2Cr_2O_7$ (0.15 M)	1.5 on (100)	4–300	
Wright-Jenkins 60 ml HF (49%) 30 ml HNO_3 (69%) 30 ml CrO_3 (5 M) 2 g $Cu(NO_3)_2$ 60 ml CH_3COOH (100%) 60 ml H_2O	1.0 on (100)	0.02–20	Not as good for dislocations, especially on (100)
Schimmel 2 HF (49%) 1 CrO_3 (5 M)	~1.8 on (100)	0.6–15 (modified Schimmel etch <0.6)	
Yang 1 HF (49%) 1 CrO_3 (1.5 M)	1.5 on (100) 1.5 on (111)	At least 0.5–20	Better for dislocations than Wright
Sopori 36 HF (49%) 1–2 HNO_3 (70%) 20 CH_3COOH (100%)	5–20 on all surfaces	At least 0.1–16	

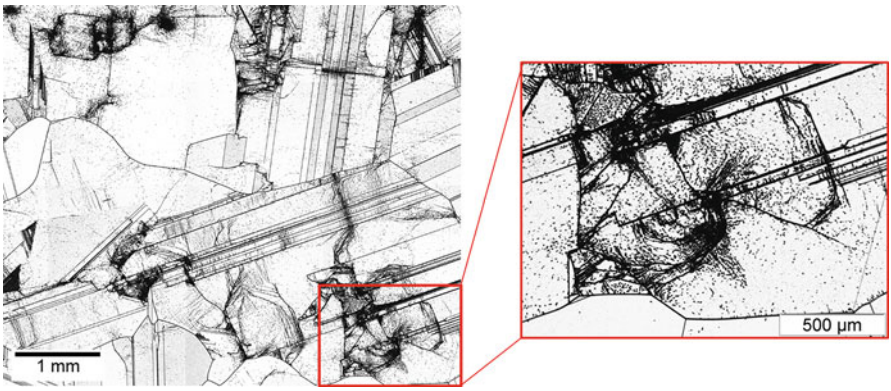

Fig. 9 Nonsymmetric grain boundaries, twins, and dislocations (e.g., etch pits in the lower right region) visible after mechanical polishing and Secco etching of a mc silicon wafer. (© Fraunhofer IISB)

The number of dislocation-related etch pits per wafer area is called *e*tch *p*its *d*ensity (EPD, unit 1/cm^2) and is an important value for characterizing the material quality with respect to photovoltaic performance (see previous chapter of this handbook).

Optical Microscopy for Local Investigation of the Silicon Sample with High Resolution

After defect selective etching, the EPDs as well as small and large angle grain boundaries can be studied by optical microscopy in the reflection mode (see Fig. 9). This method provides a resolution in µm range and is of special importance for the study of dislocations and dislocation clusters in correlation with certain types of grain boundaries. This topic will be extensively discussed in the section "Formation of grain boundaries during directional solidification (DS)".

Scanning Electron Microscopy and Transmission Electron Microscopy for Local Investigation of the Silicon Sample with Higher and Ultra High Resolution

For more detailed investigation of grain boundaries and adjacent dislocations, the Scanning Electron Microscopy (SEM) or the Transmission Electron Microscopy (TEM) can be used. These methods provide extremely high resolutions from sub-µm to sub-nm range. By use of the TEM, even the atomic structure of grain boundaries can be observed as shown in Fig. 10. The disadvantage of these methods is the quite high effort for sample preparation.

Image Processing for Evaluation of Grain Sizes and Lengths of Grain Boundaries on Full Wafer Scale

The information about the grain structure of a mc-Si sample or wafer, respectively, obtained from the reflection patterns can be improved considerably by image

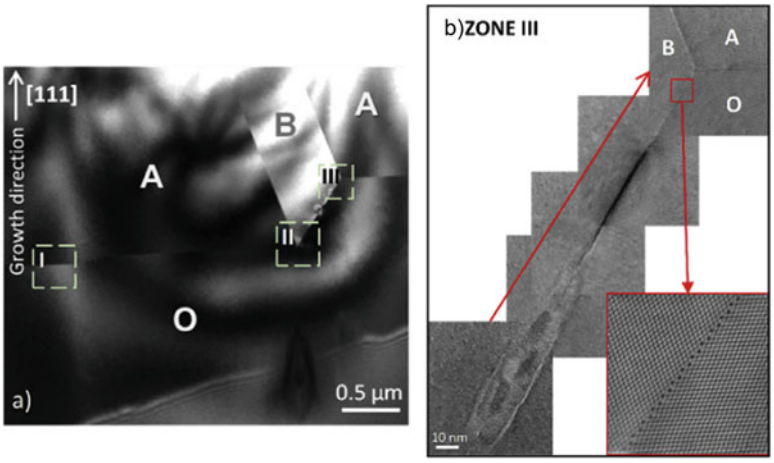

Fig. 10 (**a**) TEM image of the cross-section of a twin nucleus. (**b**) Higher magnifications of zone III of **a**: Σ9 {221} grain boundary, shown also in ultra high resolution by HR-TEM (lower square). Along the Σ9 interface, the highly distorted regions were followed by coherent (221) interfaces as shown in the HR-TEM magnification. After Oliveira et al. (2016)

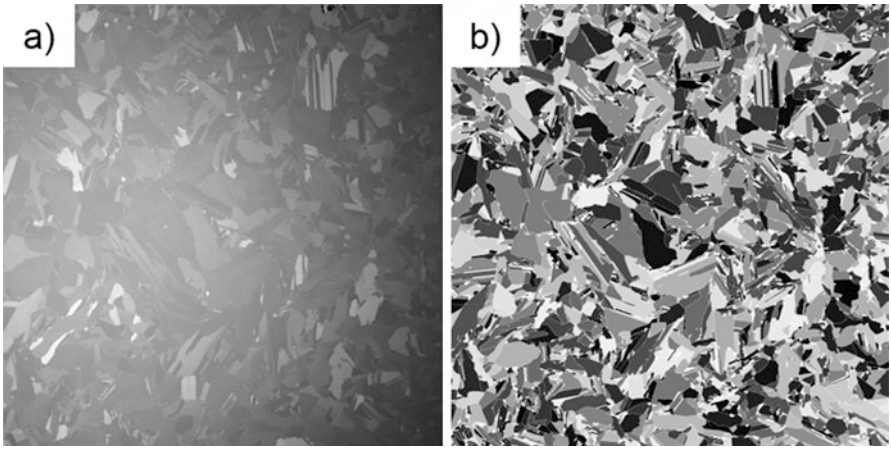

Fig. 11 Resulting images of a characterized 156 × 156 mm^2 mc Si wafer: (**a**) photograph of the investigated wafer; (**b**) detected grain structure after image processing. (© Fraunhofer IISB)

processing. In a first step, the reflection image is treated to improve the image contrast between differently oriented grains as illustrated by the example in Fig. 11.

Now a quantitative evaluation of the grain structure is possible by transforming a *gray value* image like the example in Fig. 11b into a *binary* grain image. The examples in Fig. 12 reveal now clearly the grain boundaries. It is important in this kind of image transformation to define the minimum number of pixels which represents one individual grain.

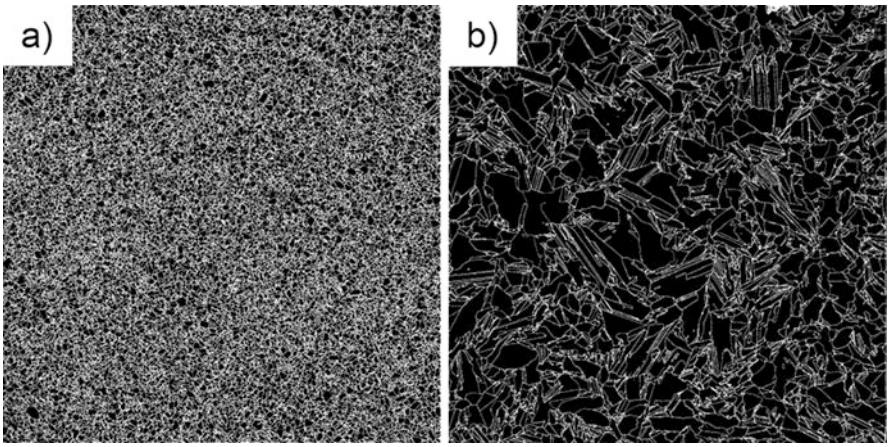

Fig. 12 Binary grain image of 156 × 156 mm^2 wafers for a fine grained structure (**a**) and a structure with large grains (**b**). (© Fraunhofer IISB)

Detailed studies in the authors group have shown that a minimum grain size of 0.05 mm^2 gives reliable results. Based on this evaluation, geometrical data can be obtained like average grain size, distribution of grain size, and length of the grain boundaries on full wafer scale. For example, the quantitative evaluation of the grain structure of Fig. 12 results in an average grain size of 1.1 mm^2 with a standard deviation of 1.6 mm^2 for the fine grain structure (a) and 6 mm^2 with a standard deviation of 16 mm^2 for the coarse grain structure (b). Obviously, the fine grain structure is more uniform than the coarse one.

Such kind of data may already be useful for the development of solidification processes and industrial fabrication of mc Si wafers. Tools for an automated grain detection as described above are commercially available (Intego GmbH 2018).

The evaluation of geometrical data of grain structures as described above can be useful but may be not sufficient for an optimization of mc-Si with respect to solar cell performance, especially if one considers the minority charge carrier lifetime. It is known from several studies and extensively discussed in this handbook that the recombination rate of the minority charge carriers is strongly increased by dislocation clusters whose formation is favored by certain grain orientations and certain types of grain boundaries. Therefore, it is necessary to include the crystallographic orientation of the grains into the characterization.

In principle, it is possible to use the dependence of the optical reflectivity from the crystallographic orientation. Sopori et al. (2011) have demonstrated that the non-isotropic KOH-etchant exposes a unique texture shape for each grain orientation which can be calibrated to provide the crystallographic orientations. It was shown that such reflecting maps of a mc-Si sample can be transformed into orientation maps.

More common and effective, however, are diffraction methods like electron beam back scatter diffraction (EBSD) and X-ray diffraction (Laue method) for determining the crystallographic orientation matrix of certain grains and relate them to their exact location within the mc "texture." (The term "texture" refers to the phenomenon of preferred crystallographic orientation of grains in a mc material).

Furthermore, the unique allocation of grain orientation *and* the correlation to its position is the prerequisite for a determination of the type of grain boundary between two neighboring grains. This topic is subject of the following section.

Orientation Mapping and Determining Grain Boundary Types

Electron Beam Back Scatter Diffraction (EBSD)

The principle of EBSD is based on the detection of electrons which are back scattered from a sample surface that is irradiated by a focused electron beam. The backscattered electrons escaping the sample surface may exit at the Bragg condition which is related to the periodic atomic lattice planes. Therefore, the diffraction pattern of these electrons, called "Kikuchi pattern," contains the information about crystallographic (grain) orientation at the position of the incident electron beam. For more details, the reader is referred to the textbook of Randle (2003).

Experimentally, EBSD is carried out in a scanning electron microscope (SEM) which must be especially equipped for EBSD. This involves the possibility of tilting the sample with respect to the incident electron beam, a detector unit consisting of phosphor screen(s), lens system, and sensitive CCD camera. The analysis of the diffraction pattern is carried out by a special pattern indexing unit. Modern EBSD systems can provide orientation maps and patterns of grain boundary types (according to CSL nomenclature). A typical result of such an EBSD analysis is shown in Fig. 13.

The big advantage of EBSD is its implementation into a SEM system which allows the use of other beneficial characterization units like cathodoluminescence (CL), wave length dispersive X-ray spectroscopy (WPS), and energy dispersive X-ray spectroscopy (EDX). These methods can provide an even deeper insight into the material properties in relation to the grain structure and/or type of grain

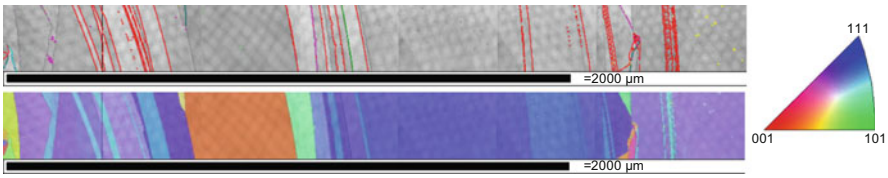

Fig. 13 Grain orientation map (below) as well as grain boundary types (above) (both color coded) obtained by EBSD measurements on a mc silicon wafer. The color of the grain boundaries relates to Σ3 (red), Σ5 (green), and R (purple). (© Fraunhofer IISB)

boundary. For more details about these methods, the reader is referred to the literature.

EBSD is nowadays the most prevalently used characterization technique for the generation of an "orientation map" of a mc-Si sample, especially in combination with the further SEM-related tools for texture analysis. The main advantage of EBSD is its high spatial resolution (~0.5–10 nm). The angular resolution is estimated to be ~0.5–1°. However, sample preparation for EBSD analysis is very time consuming because a polished sample surface with a superior quality is needed since the quality of the Kikuchi pattern is strongly dependent on the surface quality. Further, the mc-Si samples should be etched (leading again to impurities on the surface) to visualize the grain structure for the operator. Moreover, the sample size is limited to the size of the SEM sample holder, due to the large inclination angle needed between the sample surface and the incoming electron beam. As a consequence, the investigation of larger Si samples, especially a standard wafer with an area of 156 × 156 mm is not feasible by EBSD. This disadvantage of EBSD is overcome by a method using X-ray diffraction which is described in the following.

Laue Scanner Method

The so-called "Laue scanner" system was developed in the authors laboratory (see Lehmann et al. 2014). It uses the well-known X-ray diffraction technique according to the Laue method as it is common for the determination of the crystallographic orientation of single crystals. The determination of the grain orientation map of a mc-Si wafer requires a local correlation of the position of the X-ray spot and the position of the corresponding grain. The diameter of the X-ray spot can be varied between 0.3 mm and 2 mm according to the minimum grain diameter which should be considered. The spot size of the X-ray determines the signal quality, i.e., the measurement time for one Laue pattern. For example, a beam diameter of 0.3 mm results in the measurement time per Laue pattern of 20 s. The Laue pattern of each grain is detected and evaluated automatically. The sample stage (dimension 380 × 400 × 500 mm^3, maximum load 40 kg) is motorized to provide a fully automated scanning of the sample surface and allows the measurement of up to four standard size wafers (156 × 156 mm) per run. The shortest mapping time is achieved if one uses only one Laue measurement for each grain. This can be achieved by using the geometrical data of the grain structure which is evaluated from optical reflection measurements as it was described in the section "Optical Grain Detection and Analysis." In the case of the Laue scanner, these data are provided by a commercial "grain detector" (Intego GmbH 2018). The position for the X-ray spot for each grain is selected to be the geometrical location which has the largest distance to the surrounding grain boundaries. By combining all these data, it is possible to generate an image of the grain structure of a sample where the crystallographic orientation is allocated to each grain. Based on these data, a complete representation of all grain boundaries of the grain structure can be represented in the CSL notation. A typical result of a mc-Si

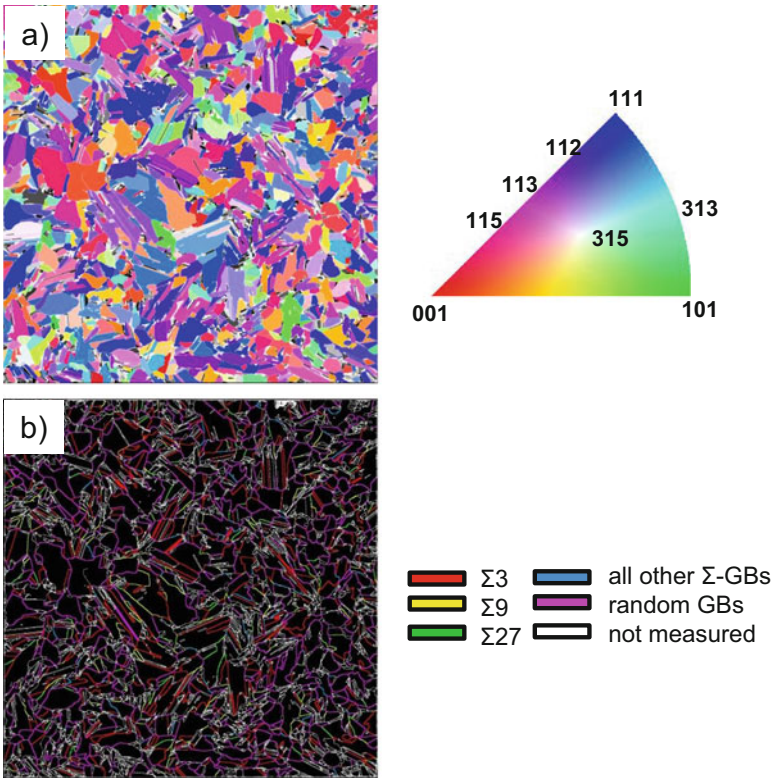

Fig. 14 Results of characterization of a 156 × 156 mm^2 mc Si wafer by the "Laue scanner" (see text). Texture map of grain orientation (**a**) and types of grain boundaries in the CSL notation (**b**). (© Fraunhofer IISB)

wafer is shown in Fig. 14. It is the same wafer which was already depicted in Fig. 11 showing the intermediate result of the "grain detector" within the complete "Laue scanner" procedure. The total time for generating the results of Fig. 14 (including Fig. 11) is about 2–5 h depending on the number of grains to be measured per wafer. For further details, see Lehmann et al. (2014).

Characterization of Electronic Material Properties in Relation to Grain Structure and Grain Boundaries

The characterization methods which were discussed in the previous sections of this chapter refer directly on the grain structure and grain boundaries with respect to their geometric parameters, crystallographic orientation or CSL type, respectively. However, electronic material properties like the spatial distribution of the minority carrier lifetime in relation to the grain structure and grain boundaries are of great interest. This section gives a short compilation of characterization methods which are in use

for analyzing these material properties. For more details, the reader is referred to other chapters in this handbook and the corresponded literature.

Photoluminescence Imaging

Photoluminescence (PL) is based on the physical effect that excess carriers in Si – generated in PL by "photo"-excitation, typically by Laser illumination – can recombine optically, i.e., by emission of light. Any defect-correlated reduction of the photo-generated excess carriers is reducing the intensity of the PL emission which can be detected directly on the wafer scale. A typical PL characterization tool consists of a couple of exciting laser diodes (emitting in the range of about 800 nm) and a light detection unit collecting the luminescence emission by a CCD camera equipped with filters to reject the laser reflected light.

Due to its very short measurement time (just a few seconds per wafer), PL is a very efficient characterization tool which can even be used for an inline wafer inspection during solar cell production. It has been shown in literature that grain boundaries and related dislocation defects, which are correlating negatively with the open-circuit voltage of a solar cell are clearly visualized in PL images (Demant et al. 2016). PL images can also reveal an increased (or decreased) local contamination of impurities by a reduced average PL intensity. Both effects are illustrated by the examples shown in Fig. 15a, b.

Similar results can be obtained with minority carrier lifetime measurements by, for example, microwave detected photoconductive decay (μ-PCD) or microwave detected photoconductivity (MDP). By stimulating the Si sample with a laser charge carriers are generated which recombine in dependence on the locally present electrical active crystal defects especially impurity decorated dislocations and grain boundaries. This recombination signal is detected by the intensity of reflected microwaves which decrease over time. As a result, the minority carrier lifetime

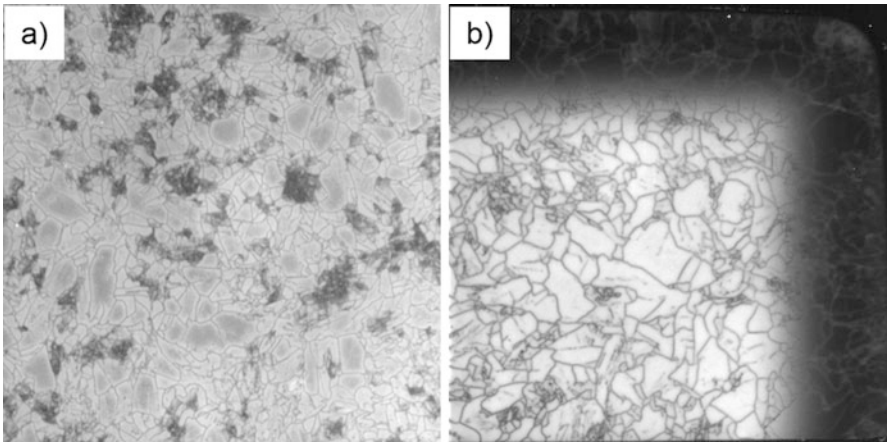

Fig. 15 PL-images of 156 × 156 mm^2 mc-Si wafers taken from the ingot center (**a**) and the ingot edge (**b**). (© Fraunhofer IISB)

is the lower the more defected and contaminated the measured sample region is. A typical lifetime-map resulting from these methods is shown in Fig. 7 on the right.

Electron Beam Induced Current (EBIC)

Electron beam induced current (EBIC) is a quite feasible method to investigate the recombination strength of grain boundaries in mc-Si material. The measurement setup is typically integrated in a scanning electron microscope (SEM) which provides a high resolution in the μm range but it is also limited with respect to the sample area which can be investigated. For the measurement, an electron beam locally induces charge carriers in the semiconducting material which are separated by a p-n- or Schottky-junction. At the ohmic contacts on both surfaces of the sample, a small current (in the range of μA to nA) can be measured in dependence on the recombination strength of the crystal defects. After mapping the sample gray value images can be produced by software in which a higher contrast corresponds to a higher recombination activity (smaller current). In Fig. 16, an example is shown where the recombination strength of different grain boundary types in mc Si silicon was measured in dependence on the iron contamination level.

Formation of Grain Boundaries During Directional Solidification (DS)

Research and development of directional solidification (DS) of Si were driven from the very beginning by the perspective of cost reduction compared to the Czochralski (CZ) growth of Si. Mainly two aspects are behind this idea. Firstly, the upscaling of the DS process is much easier compared to the CZ process. Secondly, DS provides the possibility to avoid the expensive seeding procedure with necking and conical crystal shaping of the CZ process (see, e.g., Friedrich et al. 2015) which offers for DS an up to eight times higher throughput compared to CZ (according to Lan et al. 2017).

Meanwhile several modifications of the DS process were developed. This chapter provides a detailed comparative consideration of the various variants of the DS process and its results with respect to the formation of various types of grain boundaries including dislocation defects.

Previously, it was already shown how grain boundaries can influence the quality of mc-Si. It was also shown that the formation and multiplication of dislocations depend strongly on the occurrence of certain types and structures of grain boundaries. Based on this knowledge, one can formulate the following goals for the formation of a favorable grain structure in a DS process of mc Si:

(i) As much as possible large grains which means a few grain boundaries, in the ideal case only one single grain, i.e., a monocrystal
(ii) Preferably grain boundaries which are electrically harmless; this holds especially for twin boundaries, e.g., type Σ3.

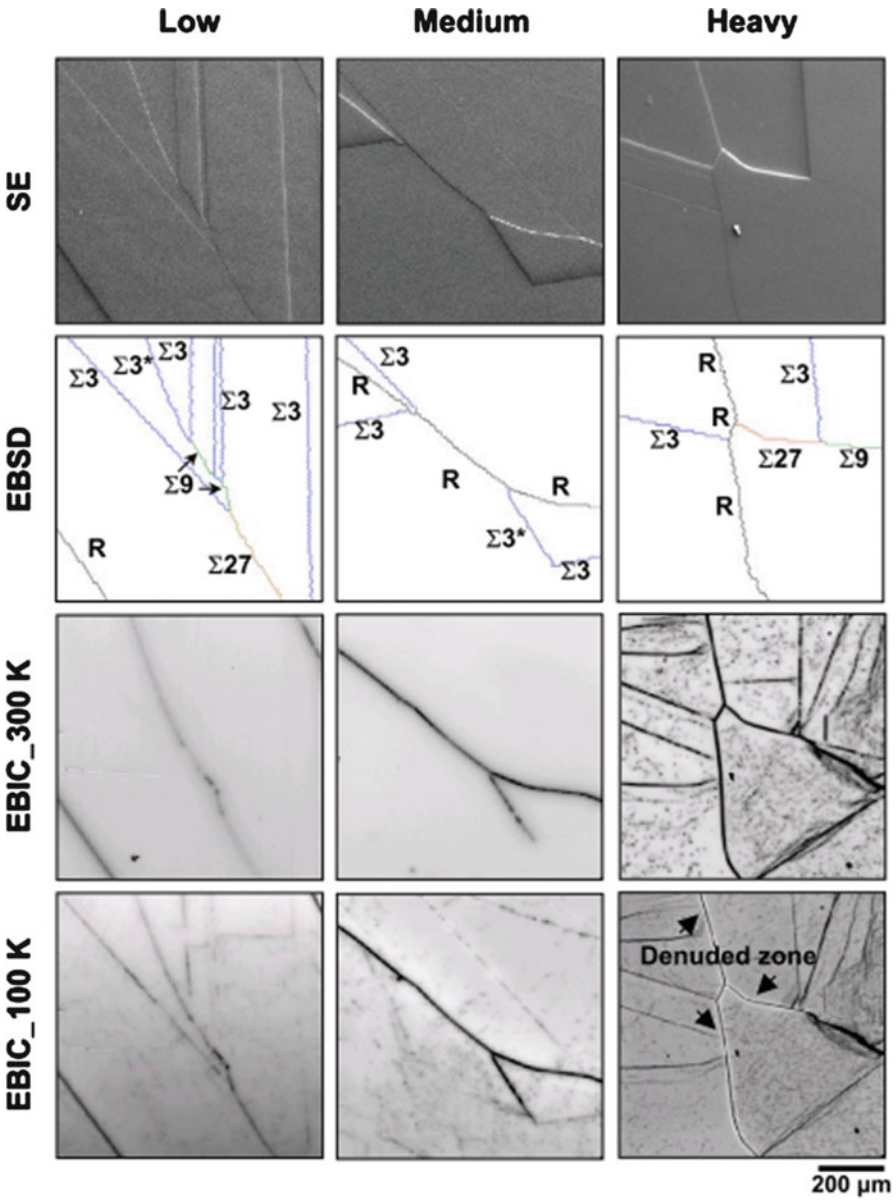

Fig. 16 Local SE(M), EBSD, and EBIC images of different grain boundaries in mc-Si wafers which are low, medium, and heavy iron contaminated. The SE(M)-images show the GB structure, the EBSD images the GB type, and the EBIC images the electrical activity of the grain boundaries. After Chen et al. (2007)

(iii) As few as possible dislocations which means preferably grain boundaries which do not provoke the generation of dislocations, i.e., grain boundaries with low stress (congruent grain boundaries). Furthermore, the grain boundaries should impede the movement and multiplication of dislocations; this holds especially for random (R) grain boundaries, whereas twin boundaries (like Σ3) are not impeding the movement of dislocations.

The outcome of the objectives i, ii, iii cannot be a unique strategy to achieve high quality of the mc material because the objectives are partly contradictory. In fact, it turns out that different strategies can be successful. In each of these routes, the nucleation at the beginning of the crystallization process plays an important role.

In the beginning of the DS process development, one tried to achieve a material with as much as possible large grains (i). Here, the nucleation respectively the seeding process is initiated as usually in a DS crystal growth process by decreasing the temperature of the totally melted Si feed material with the lowest temperature at the crucible bottom. The seeding crystallization itself is beginning by a heterogeneous nucleation at the surface of the crucible coating (standard is silicon nitride (Si_3N_4)) of the flat crucible bottom. The Si_3N_4 coating is necessary to avoid the sticking of Si at the silica crucible and to reduce contamination from the crucible walls. This seeding process which results in a large amount of less harmful twin boundaries (ii) will be called further as *"classic mc."*

A further coarsening of the grain structure, i.e., increase of the grain size can be achieved by an improved thermal processing during the initial seeding phase with regard to a higher supercooling of the melt. This effect causes the preferential formation of dendrites at the crucible bottom. Therefore, this seeding process will be called further "dendritic" (▶ Chap. 8, "Growth of Multicrystalline Silicon for Solar Cells: Dendritic Cast Method"). Both the "classic mc" and "dendritic" DS processes will be discussed in detail in section "Coarse Grain Structures Without Seed Crystals (Classic mc and Dendritic mc)."

In order to generate an even more "coarse" grain structure with the final goal of large monocrystalline ingot regions, a seeding variant with Si monocrystal seeds was developed. The principle idea of this technology is to combine the cost benefit of DS growth with the high material quality of monocrystalline Si in order to provide a more cost effective mono Si in comparison to CZ material. For that purpose, monocrystalline Si seed plates, cut from CZ ingots, are placed at the crucible bottom in order grow a monocrystalline ingot without any grain boundaries and also few dislocations (i + iii). However, this technology exhibited a lot of challenges like the formation of grain boundaries at the ingot periphery or the formation of small angle grain boundaries within and above the joints of the seed plates. This so-called "*quasi-mono" silicon* (QM) was for several years in the worldwide focus of the Si DS research and development (▶ Chap. 9, "Growth of Crystalline Silicon for Solar Cells: Mono-Like Method"). A more detailed

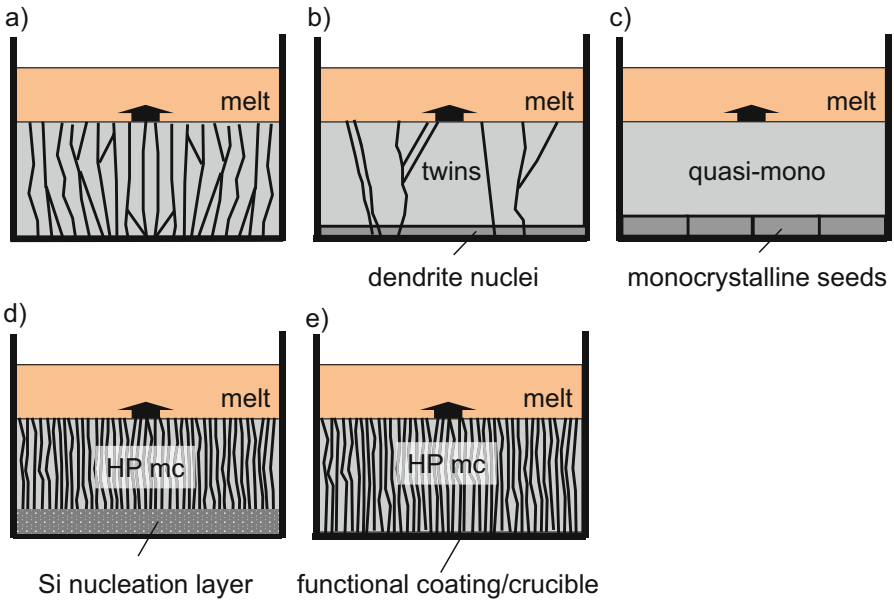

Fig. 17 Schematic representation of the five important seeding variants which are used to control the formation of the grain structure in the DS of Si: classic mc (**a**), dendritic mc (**b**), quasi-mono (**c**), high performance mc (**d**), and high performance mc 2.0 (**e**). For details, see text

description is given in section "Towards Monocrystals by Using Monocrystalline Seeds (Quasi-Mono QM)."

In the course of further research and development of mc-Si growth, it was surprisingly found that a fine grained texture, i.e., small grain sized mc-Si resulted in solar cells with higher efficiencies compared to cells made from classic mc and dendritic mc. This kind of material was henceforward called *"high performance mc Si"* (HPM) (► Chap. 7, "Growth of Multicrystalline Silicon for Solar Cells: The High-Performance Casting Method"). The fine grained texture of the HPM material contains a high number of random (R) grain boundaries which are impeding the movement of dislocations (iii). These structural conditions can be achieved by various alternative seeding methods. One possibility is to use a fine grained Si feedstock material as a seeding layer. This option needs a careful melting procedure of the feedstock in order to leave a residual layer of not melted Si for seeding (see section "Fine Grain Structures with Seeding on Si Feedstock (Original HPM)."). Such a bit difficult step can be omitted if the coating surface of the crucible bottom can provide nucleation conditions for a fine grained texture. The results of this recent development (named *HPM 2.0*) are presented in section "Fine Grain Structures without Seeding on Si Material (HPM 2.0)."

Figure 17 shows a schematic representation of the five variants of seeding procedures in the DS of Si which will be discussed in the following.

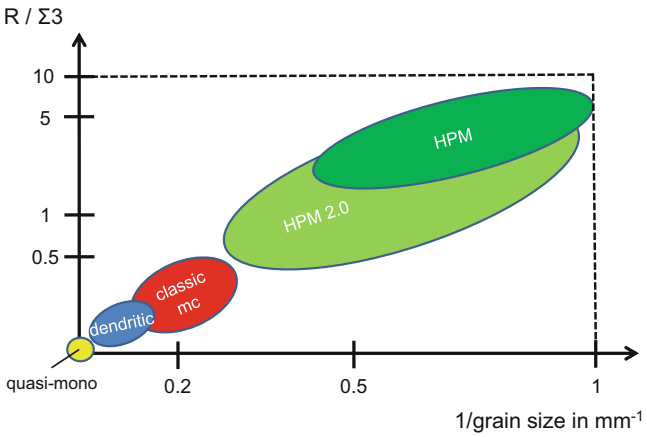

Fig. 18 Ratio of random to twin grain boundaries R/Σ3 (logarithmic axis) versus the reciprocal grain size for the different silicon materials grown by various variants of the DS method (see text)

Figure 17(a) represents the classic mc Si without any precautions for seeding, (b) illustrates the variant with dendrite formation on top of the crucible Si_3N_4 coating layer, (c) shows the quasi-mono method of seeding with monocrystalline seed crystals which comes closest to the single crystal growth of other materials like GaAs by the DS technique, and (d) and (e) display the two variants of the high performance mc material: firstly, the use of a fine grained layer of Si feedstock material which needs a comparable melting process like the quasi-mono approach (d) and secondly, the use of a specially prepared incubation surface of the Si_3N_4 coating or the crucible (e).

Figure 18 provides a graphical presentation of the different types of grain structures resulting from the DS variants sketched in Fig. 17. The ratio of the number of random (R) to twin (Σ3) grain boundaries is plotted versus the grain size (reciprocal). The five technological approaches *classic mc, dendritic, quasi-mono, HPM, and HPM2.0* are represented in the diagram and will be discussed in detail in the following sections.

Coarse Grain Structures Without Seed Crystals (Classic mc and Dendritic mc)

In the DS processes without seed crystals, it is obvious that the formation of the grain structures, i.e., grain orientation, grain size, type of grain boundaries, as well as the formation of dislocations is decisively influenced by the initial process of self-seeding at the crucible bottom. This so-called heterogeneous nucleation means that the first Si nuclei are forming in contact with the surface of a dissimilar material, in this case the Si_3N_4 layer which is coating the inner surface of the SiO_2 crucible.

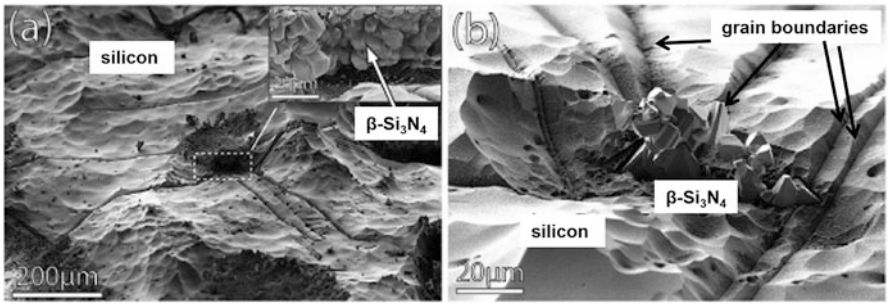

Fig. 19 (**a**) SEM images of the bottom surface of a mc silicon ingot after Sopori etching which has removed almost the complete residual Si_3N_4 coating. (**a**) Shows regions of physical contact between the particle-layer and the solidified silicon. (**b**) Facetted beta Si_3N_4 particles which are embedded into the silicon. After Ekstrøm et al. (2016)

The conventional or *classic DS process* developed in the late 1980s uses standard silica crucibles with a spray coated layer of Si_3N_4. The main purpose of this Si_3N_4 layer is to prevent the sticking of the solidified silicon with the silica crucible wall. Instead of sticking at the silica wall, the solidified Si material sticks more or less at the Si_3N_4 coating which separates during cooling from the silica wall depending on its properties. At the end of the cooling process also, the Si_3N_4 powder can be easily removed from the Si block. Ekstrøm et al. (2016a) studied the nucleation process of Si directly on the Si_3N_4-coating more in detail (compare Fig. 19). Typically, Si_3N_4-powder containing the crystallographic alpha phase is used for the crucible coating. Due to dissolution of Si_3N_4 and transfer of a dedicated amount of nitrogen into the liquid silicon (until the local solubility at elevated temperatures is reached), hexagonal beta Si_3N_4-particles are formed on top of the alpha phase based crucible coating. It is assumed that the initial Si nucleation takes place at the facets of this hexagonal beta Si_3N_4-precipitates. Because the Si nuclei are preferably growing at the hexagonal side, facets of the Si_3N_4 most preferably Σ3 grain boundaries were formed.

At this point, the focus will be directed phenomenologically to the formation and development of the grain structure which results from the initial seeding. As soon as the initially isolated nuclei have been grown laterally to a length that they touch each other, the first grain boundaries are generated. Now the crucible bottom respectively the coating is covered by a complete layer of mc Si. During the further growth of this layer, various mechanisms and phenomena can influence the grain growth and hence the formation of grain boundaries:

- Grains with certain crystallographic orientations are growing preferentially (due to the differences in the surface energies depending on the crystallographic orientation) (see the example in Fig. 20)
- Grain boundaries with a low energy are preferentially growing. This holds especially for the twin Σ3 boundary (see Fig. 21).

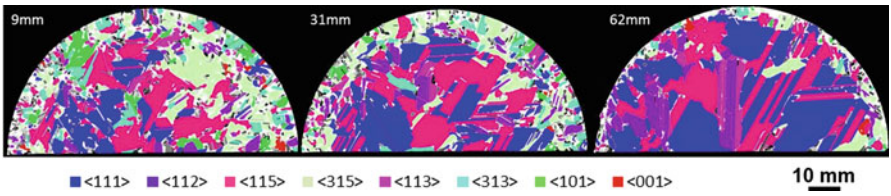

Fig. 20 Examples of the growth of grains with a preferential orientation (<111>, <115>, and <112>): sections perpendicular to the axis of solidification at three different heights (9, 31, and 62 mm) of a G0 ingot. (© Fraunhofer IISB)

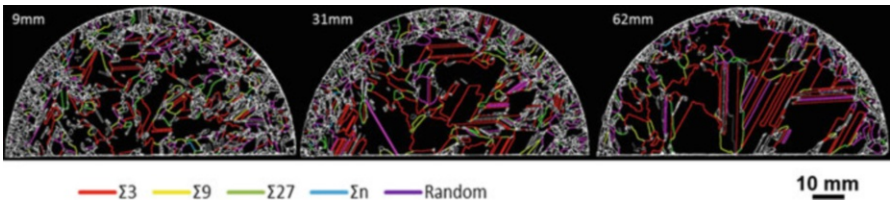

Fig. 21 Examples of the growth of grains with preferential twin boundaries (Σ3): sections perpendicular to the axis of solidification at three different heights (9, 31, and 62 mm) of a G0 ingot. (© Fraunhofer IISB)

- Grain boundaries with a high energy can be converted into grain boundaries with a lower grain boundary energy (compare Fig. 6).
- Dislocations are present a priori along small angle grain boundaries (see below Fig. 28).
- Dislocation lines are spreading across certain grain boundaries, like Σ3 (see, e.g., Fig. 22 left).
- Dislocation lines can be blocked by certain grain boundaries (see, e.g., Fig. 22 right).
- Dislocations can be generated by grain boundaries with a high stress caused by incoherency of the adjacent lattices (see, e.g., Fig. 23).

The grain structure resulting from the *classic mc* process is a resulting mixture of all the phenomena specified above. It has typically an average grain size of $\geq$4 mm^2 and a fraction of R-type boundaries to Σ3 boundaries between 0.5 and 0.25 (compare Fig. 18).

Figure 24 shows an image of such a grain structure. One characteristic feature of this structure is the preferred elongation of the grains along the direction of growth or solidification, respectively. It is also obvious from Fig. 24a that certain grains have a preferred growth and are "overgrowing" other grains.

A generally observed problem of this grain structure is the occurrence of grains with a very high dislocation density (EPD $\geq 10^6$ cm^{-2}), as shown in Fig. 24b. The PL image illustrates the deleterious effect of the dislocations by the strongly reduced PL intensity. There are hints in the literature that the generation of dislocations could

be provoked by the stress generated by the formation of incoherent type R grain boundaries, see, e.g., Fig. 23 or Ryningen et al. (2011).

In summary, the resulting grain structure discloses the advantages as well as the problems of the classic mc material with respect to the performance of solar cells. Relatively large grains are meaning a low number of harmful grain boundaries. The Σ3 grain boundaries with its high percentage do not act as recombination centers for minority charge carriers. However, Σ3 grain boundaries are also not acting as barriers for the transition of dislocations lines (compare Fig. 22 left). Dislocations which are emitted from the regions with a high dislocation density are not hindered by Σ3 grain boundaries. Therefore, the classic mc material with its large areas of high dislocation density has decisive limitations with respect to an application of high performance solar cells.

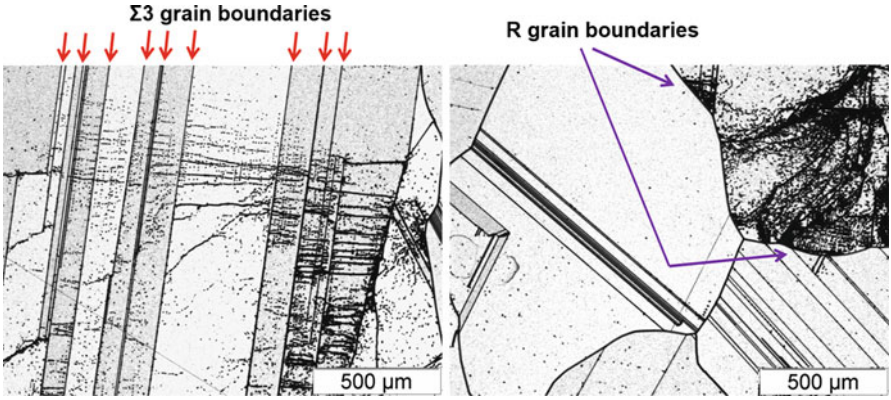

Fig. 22 White light microscopy images of dislocation lines which are: (left) spreading across Σ3 twin boundaries and (right) blocked by R-type grain boundaries. (© Fraunhofer IISB)

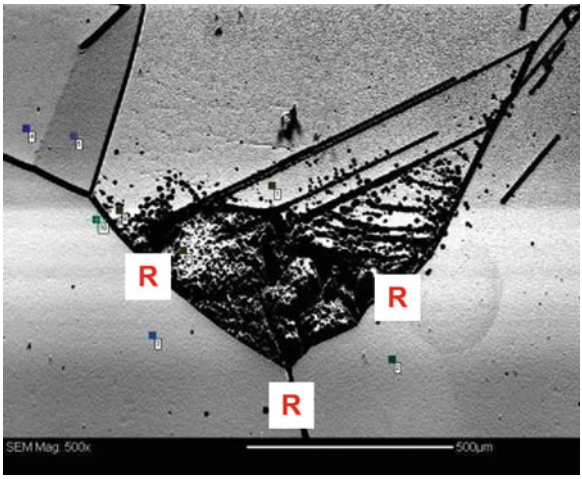

Fig. 23 SEM picture of R-type grain boundaries with adjoining region of high dislocation density. The boundary triple junction seems to be the source of the dislocation formation (incoherency). (© Fraunhofer IISB)

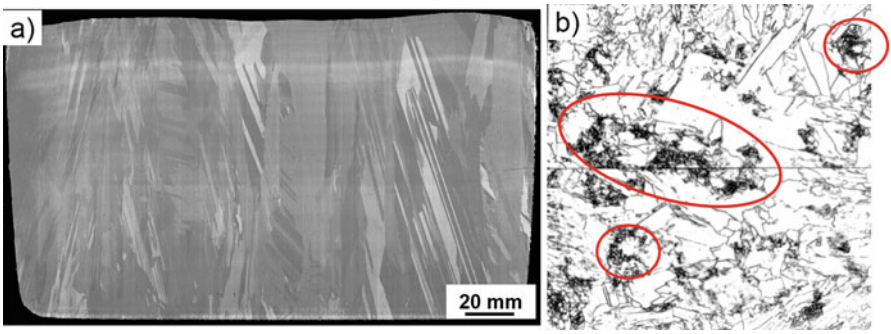

Fig. 24 (**a**) Grain structure image of a vertical section parallel to the direction of solidification of a G1 size ingot processed according to the "classic mc" conditions. The typical coarse structure with elongated grains and twins is visible. (**b**) PL-image of a 156 × 156 mm^2 wafer perpendicular to the growth direction at 80 mm height of the same ingot with areas of high dislocation density (inside marked regions). (© Fraunhofer IISB)

One strategy to overcome the problems of dislocation clusters is to decrease the number of incoherent grain boundaries by a distinct increase of the grain size.

The publication of Fujiwara et al. (2006) was one of the first reports about a successful coarsening of the mc grain structure by an "improvement" of the classic mc process. This improvement consisted mainly in an increase of the supercooling at the beginning of the seeding step followed by an increased rate of solidification. Both measures are causing the formation of dendritic nuclei in the seeding phase and its growth in both directions, lateral on the surface of the Si_3N_4 coating and perpendicular to it. A typical example of the resulting grain structure is shown in Fig. 25 where the increased grain size is clearly visible.

The basic cause of the dendrite formation is the relatively high supercooling ($\geq$10 K) of the Si melt at the crucible bottom. This supercooling is possible due to a poor wetting of the Si_3N_4 surface by Si. Studies of Fujiwara et al. (2006) and Nakajima et al. (2010) have shown that the dendrites are growing parallel to the crucible bottom with the preferred crystallographic orientations <110> and <112>. The preferred orientations of the growth interfaces in the direction of solidification are the (112) and (110) planes, respectively. These relatively large elongations of the dendrites are causing the large grain sizes (up to several centimeters) at least for the firstly solidified portions of the ingot. The grain structure is characterized by a very high portion of Σ3 grain boundaries up to 80% (equals to $R/\Sigma3 < 0.25$, see Fig. 18) which result from the uniform dendrite orientation. More details like the selection of competing grain growth in dependence on process conditions (cooling rate, shape of growth interface, rate of solidification) are discussed by Lan et al. (2012).

Solar cells which were fabricated from dendritic mc-Si show cell efficiencies which are increased by nearly 1% in comparison to classic mc Si according to Nakajima et al. (2010). Despite of the positive results of the dendritic mc material, it did not prevail in industrial production. This had several reasons: the conditions for the high super-cooling which is essential for the formation of the initial dendrites

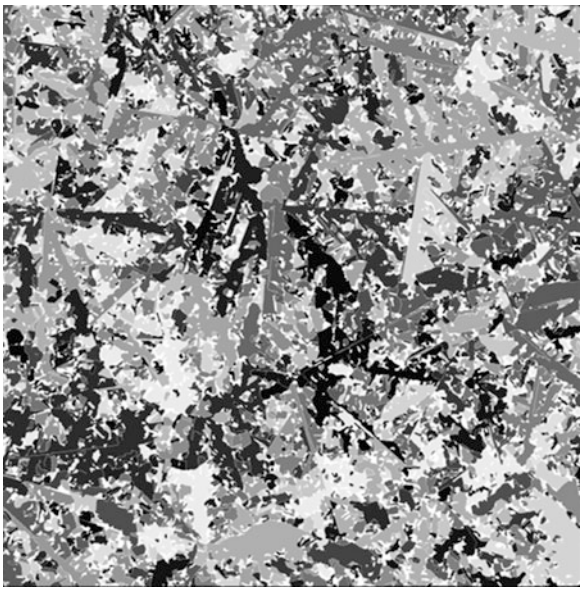

Fig. 25 Image of a typical dendritic grain structure of a bottom near 156 × 156 mm^2 wafer of a G1 ingot which was grown with higher cooling rates in comparison to the classic mc. (© Fraunhofer IISB)

are difficult to be provided reproducibly. The necessary high cooling rates at the beginning of the solidification step pose a certain risk for a breakage of the crucible and its containment. Furthermore, the grain structure of the mc material itself has the disadvantage that its heavily twinned texture does not prevent the spreading and multiplication of dislocations. In consequence, the benefit of the dendritic structure is lost after some centimeters of growth. Finally, according to the author's results, it seems doubtful whether a successful upscaling beyond ingot heights of 300 mm with the growth of large grains with only few dislocations could be possible.

A further improvement of the material quality by increasing the grain size is possible by using monocrystalline Si seeds. This will be the subject of the following section.

Towards Monocrystals by Using Monocrystalline Seeds (Quasi-Mono QM)

The idea of the q*uasi-mono (QM)* technology was not new in the end of 2000s when it has come into the field of interest of nearly all Si wafer producers who dealt with the directional solidification technique. The use of a monocrystalline Si plate which is placed at the crucible bottom (see Fig. 17c) in order to grow in the best case a real monocrystal or at least an ingot with only a few grain boundaries ("quasi-mono") was firstly published in the end of the 1970s by Schmid (1975) and Helmreich (1980). However, a serious development of this technology for producing industrial Si monocrystals for PV application has started only in 2007 (Stoddard 2009; Stoddard et al. 2008). The main nominal benefits in comparison to the *classic* mc or *dendritic mc* Si as well as the mono CZ-material are:

(a) A higher wafer quality due to the absence of crystal defects like grain boundaries and dislocations (i.e., approaching the structure and properties of CZ-Si)
(b) Better light capturing properties after alkaline texturing due to its uniform <100> surface orientation (at the same level as CZ-Si)
(c) A lower oxygen content compared to CZ-Si
(d) Less production costs in comparison to the more cost intensive monocrystalline CZ-material

All of these benefits should make the QM material to be competitive, to be better, or even to replace the mono CZ-Si for PV application. However, it turned out pretty soon that the growth of a 100% monocrystalline ingot by this technique is rather complicated. In the following, the main problems or tasks, respectively, during the growth of QM Si material are listed:

(a) *Seeding control*: Analogue to the HPM technology (see section "Fine Grain Structures with Seeding on Si Feedstock (Original HPM)"), it has to be taken sure that the monocrystalline seed plate is partly melted but not completely melted. This means a more complicated seeding processes in comparison to the *classical mc* approach (Camel et al. 2009).
(b) *Parasitic nucleation at crucible walls*: In contrast to a CZ crystal, the ingot in a DS process grows in contact with the crucible side walls. Here heterogeneous nucleation can take place in the same way as during the classic mc growth. This results in the growth of a multigrain structure in the regions of the side walls which reduces the monocrystalline ingot volume (Trempa et al. 2012).
(c) *Dislocation formation within the bulk and/or the surface of the monocrystalline seed plate*: Dislocations can be formed during heating up within the seed plates due to thermal stress and/or mechanical load of the feedstock on top and can propagate into the grown ingot volume (Trempa et al. 2016). See Fig. 26.
(d) *Formation of small angle grain boundaries (SAGB) and dislocations at the seed joints*: According to the crystallographically non-exact aligning of the seed plates, SAGBs and subsequently dislocations are formed and spread into the ingot volume (Trempa et al. 2014).
(e) *Iron contamination of the seed crystals – means increased bottom "red zone"*: The original "high purity" seed plates cut from CZ ingots are contaminated with metals, e.g., iron, already during the heating phase which is leading to an enhanced contamination of the bottom region of the QM Si ingot (Trempa et al. 2015a).

Two of these problems (b and d) will be treated in the following in more detail because they are directly correlated to the occurrence of unwanted grain boundaries within the QM material.

Concerning the parasitic grain growth at the crucible walls, it could be found that it is determined by two mechanisms, see, e.g., Trempa et al. (2012). Firstly, the

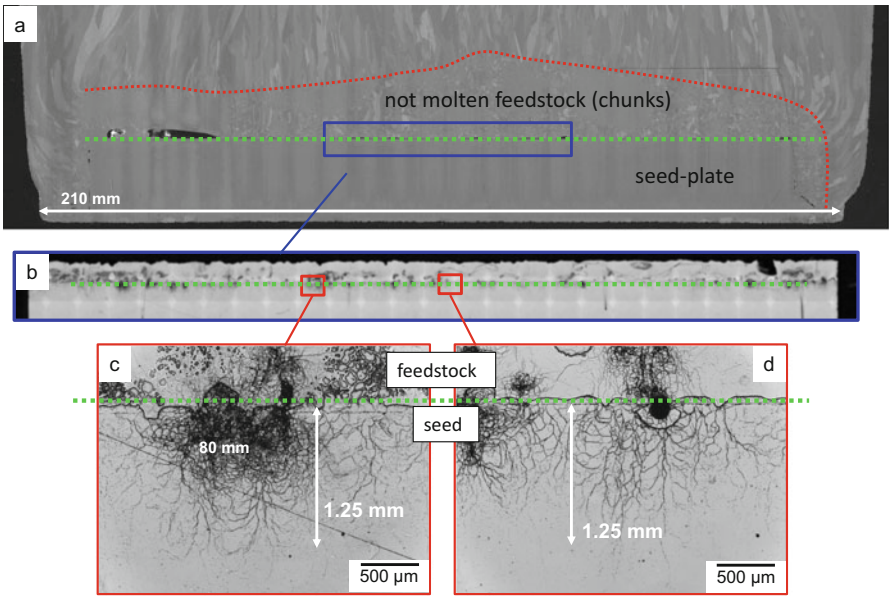

Fig. 26 Vertical sections parallel to the direction of solidification of an G1 ingot grown by using a monocrystalline seed plate (upper surface is marked by the dotted green line) and Si chunks as feedstock material. (**a**) Grain structure image of the bottom part of the ingot showing the seeding interface (curved dotted red line) which is unintentionally laying within the feedstock material. (**b**–**d**) White light microscopy images of the interface between the seed plate and the unmelted chunks (dotted green line) revealing the dislocation arrangements (**c**, **d**) which are caused by the indentation of particle tips. After Trempa et al. (2016)

classical mc-grain nucleation occurs at the Si_3N_4 coating at the crucible walls or at the outer bottom regions where no seed crystals are placed. Secondly, a twinning process occurs at the edges of the monocrystalline Si seed plates itself. Both phenomena are illustrated in Fig. 27 which shows a grain orientation mapping of an industrially grown QM Si wafer taken from an edge brick. It can be seen that the twin orientation <221> (bright blue) is directly connected to the seed orientation <100> (red), whereas the nonuniformly oriented mc grain structure which is induced by the crucible coating is located in the most outer wafer regions.

Two approaches were studied in order to overcome this problem. The most frequently used one is to adjust the shape of the solid-liquid-phase boundary in the edge regions to be of slightly convex shape in order to achieve a preferred growth direction of the mc-grains towards the crucible walls. So the range of the mc-grain growth can be limited to a size of a few millimeters. The avoidance of the formation of twins is rather difficult and cannot be solved by only adjusting the phase boundary shape. Hence, a second approach was proposed by Kutsukake et al. (2013). They found out that the use of so-called "functional grain boundaries," which are induced by seed crystals with a certain lateral orientation in the periphery regions of the ingot, can avoid the inclining growth of Σ3 twin boundaries. The extra seed near the

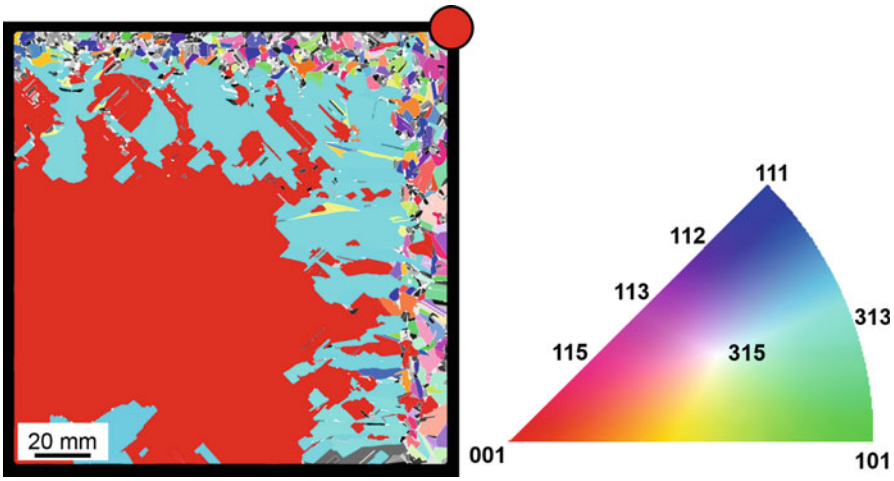

Fig. 27 Orientation mapping of an industrially grown 156 × 156 mm^2 QM Si wafer from an edge brick (left). The red dot marks the edge position of the G5 ingot. The colors represent the grain orientation according to the Euler triangle (right). After Trempa (2014)

crucible wall is blocking the Σ3 twin boundaries by the aid of a Σ5 grain boundary. This technique was successfully demonstrated for ingots with 400 mm edge length corresponding to a G3 scale by Kutsukake et al. (2014).

The other challenge in the growth of high quality QM Si ingots is the formation of dislocations at the seed joints. Due to the fact that no monocrystalline seed plates in dimensions of ~1m^2 are available from Cz-growth or other techniques, the industrial producers have to use an arrangement of several seed plates which are placed directly to each other on the crucible bottom like floor tiles, sometimes called "split seeds." The gaps between the split seeds are growing together within or just above the gaps by forming small angle grain boundaries (SAGB). The cause for the SAGB formation is the very small (unavoidable) mismatch of both Si lattices of the two neighboring seed plates by $<1°$. These SAGBs are forming an array of dislocations along the direction of solidification in the region above the seed joints. The dislocations multiply and widely spread into the ingot volume as it is shown by the microscopic views of an etched lab-scale sample in Fig. 28 as well as by PL images of a G1 ingot in Fig. 29. In consequence, the material quality and finally also the cell efficiency was even worse in these dislocated ingot regions.

A lot of investigations were made by different researchers in order to solve this problem. However, it was found that even very careful positioning of the seed plates or a chemical surface treatment of the side faces does not lead to good results. Finally, it was found that even very small relative misorientations between two adjacent seeds below 1° still result in a tremendous dislocation formation (Trempa et al. 2014; Trempa 2014; Oliveira et al. 2014; Ekstrøm et al. 2015). Only if the mismatch could be kept $<0.1°$, the dislocation formation could be significantly reduced. However, this condition is quite difficult to be reproducibly achieved in

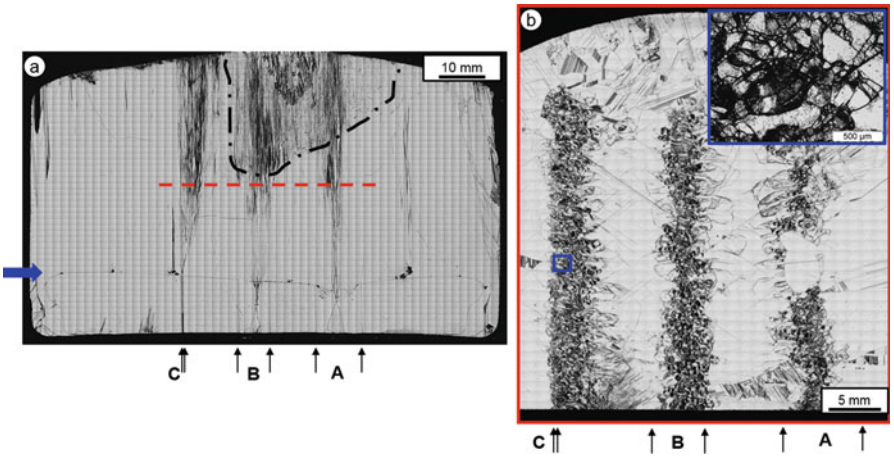

Fig. 28 Optical micrographs of a Jenkins-etched *vertical* (**a**) and *horizontal* (**b**) cut. The axial seed orientation and the gap planes are <110> and {100} oriented. The arrows at the bottom of (**a**) depict the seed edges which define the gap width A (~10 mm), B (~5 mm) and C (<1 mm). The bold blue arrow at the left periphery shows the position of the seeding interface. The red dotted line marks the vertical position of the horizontal cut shown in (**b**). The arrows at the bottom of the horizontal cut (**b**) depict the original seed wall positions. After Trempa et al. (2014)

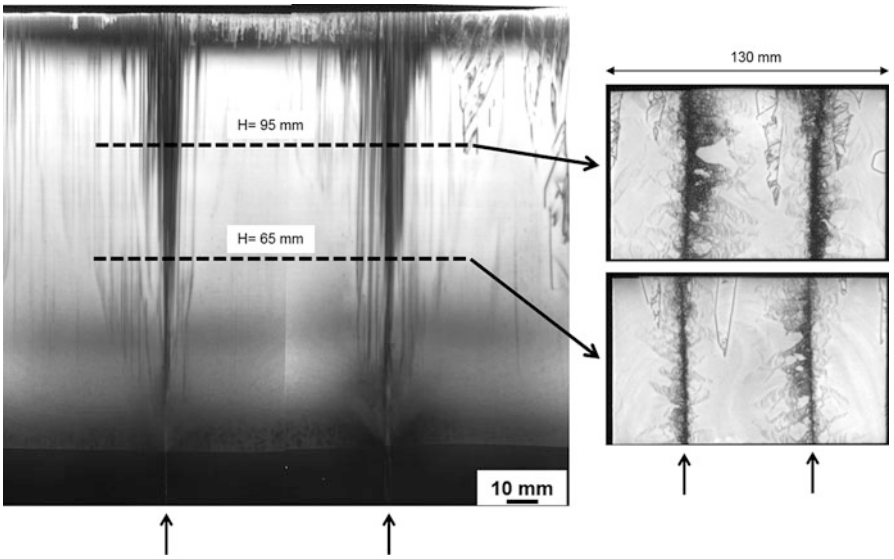

Fig. 29 PL images of vertical and horizontal sections cut from a G1 quasi-mono Si ingot parallel (left) and vertical (right) to the growth direction. The seeds joints are marked by arrows. (© Fraunhofer IISB)

an industrial production environment. One practical option could be to use rectangular seed plates instead of squared ones to reduce the number of gaps and to be very careful during seed preparation and positioning.

Grain Boundary Engineering

The problem of the slightly misoriented "Σ1" or SAGBs, respectively, with its related dislocation cascades can be overcome by using alternative orientations of the split seeds which are not causing SAGBs but certain types of large angle grain boundaries that do not result in the formation of dislocations. This alternative approach was firstly proposed by Trempa et al. (2015b) in a laboratory scale. It was found that the more nonsymmetric the grain boundary is, the less dislocations are formed. For example, a Σ33 grain boundary or a R grain boundary prohibit the formation of dislocations whereas a nonperfect Σ3 twin grain boundary induces a high amount of dislocations. Figures 30 and 31 illustrate these results.

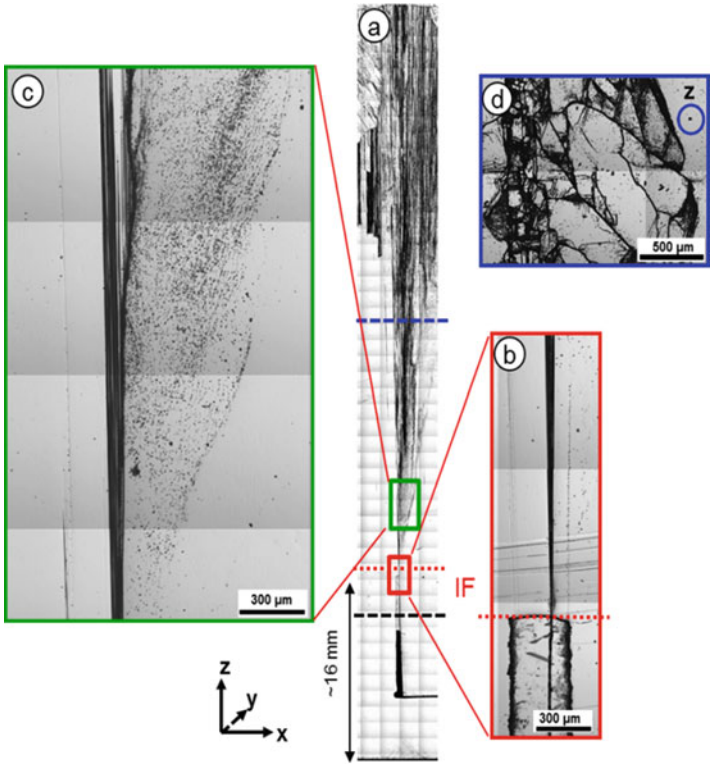

Fig. 30 (**a**) Optical micrograph of the grain boundary region of an etched vertical cut ranging from the crystal bottom to the top. The area (rectangle) close to the horizontal seeding interface (IF, red dotted line) is shown in a higher magnification in (**b**). The grain boundary structure at 50% of the crystal height (dashed blue line) is illustrated in (**d**) by a section of a horizontal cut. The area within the bigger green rectangle in (**a**) is shown in (**c**) in a higher magnification. After Trempa et al. (2015b)

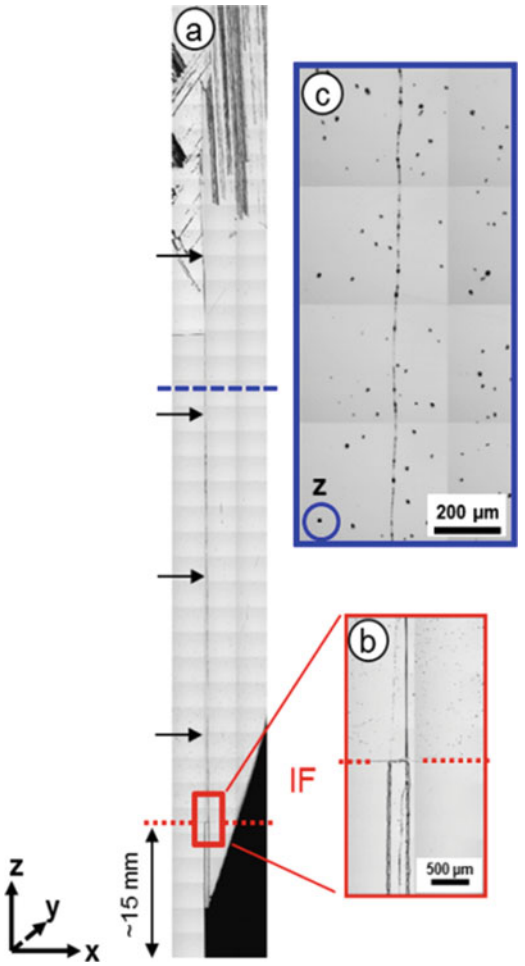

Fig. 31 (**a**) Optical micrograph of the Σ33 grain boundary region of an etched vertical cut ranging from the crystal bottom to the top. The area (red rectangle) close to the horizontal seeding interface (IF, red dotted line) is shown in a higher magnification in (**b**). The grain boundary structure at 50% of the crystal height (dashed blue line) is illustrated in (**c**) by a section of a horizontal cut. The area within the bigger green rectangle in (**a**) is shown in (**c**) in a higher magnification. After Trempa et al. (2015b)

For practical use of this method, it has to be noticed that the various seed plates have to reveal different orientations. Hence, in case of an industrial application, a large amount of seed material is needed which must be cut from CZ crystals in directions which are diagonal to the cylinder (growth) axis. This means considerably increased expenses for an industrial production. Secondly, for securing the beneficial texturing effect of a homogeneously oriented material in growth direction, the orientation of adjacent seed plates should be identical parallel to the growth direction (typically <100>).

Considering these items, Hu et al. (2015) presented the approach to induce large angle grain boundaries by rotating the seed pieces around their vertical axis by keeping the <100> growth orientation. It was demonstrated in G5 ingot dimensions (870 mm edge length) that by keeping intentional twist angular deviation of 10–45° of the adjacent seeds, the formation of dislocation and SAGBs could be almost

completely suppressed. In consequence, the defect-related areas in the whole ingot could be significantly reduced resulting in higher solar cell efficiencies of +0.6% absolute.

An alternative approach also considering the above listed items is the so-called "SMART"-approach (seed manipulation for artificially controlled defect technique) firstly proposed by Takahashi et al. (2015) where two very narrow seed pieces of different orientation are placed between the large regular seed plates which exhibit the original orientation. Instead of one, now three grain boundaries were introduced. The middle one is intentionally configured as a small angle grain boundary generating dislocations in order to reduce the stress in the ingot. The two outer ones are configured as large angle grain boundaries which should prohibit the internal generated dislocations and do not emit such by itself. However, also here several times it is observed that the large angle grain boundaries are growing diagonally and annihilate each other or enlarge the area with the unfavorable second orientation, respectively.

In summary, the material which can be produced by this technology is not really a monocrystalline material but more a "Quasimono"-crystalline (QM) material containing SAGBs and dislocations. Therefore, good QM material can only be an alternative to mono CZ-Si, but cannot replace it. Actually, the worldwide activities in the field of the QM technology are nearly completely shut down. The main reason might be the described dislocation formation above the seed joints which could not be avoided under conditions which are adequate from technical and economical point of view to an industrial production, so far. However, there are still companies working on this technology. Another reason why the work on QM processes was reduced a few years ago is the emergence of a new mc Si material type within the last years which is called "high performance mc-Silicon" (HPM) and reveals similar material properties like the QM-Si (Kutsukake et al. 2015). The HPM material including its production technologies are described in detail in the next two sections.

Fine Grain Structures with Seeding on Si Feedstock (Original HPM)

Since the year 2011 it was reported in the literature that mc Si with an average grain structure of 1–4 mm^2, which is considerably smaller than classic mc, yields in a notable increase of cell efficiencies up to 1% (Yang et al. 2015; Lehmann et al. 2016). Because of this improvement, the fine-grained PV Si is denoted since that time as *"high performance mc silicon"* (HPM).

The first HPM resulted rather accidentally during the development of the dendritic casting method. It was found by Lan et al. (2012) that certain undercooling rates, which are between that of the classic mc and the dendritic mc, are leading to a fine grained structure at the bottom end of the ingot as well to a reduced dislocation density over the ingot height. However, the process window providing the slight undercooling which is required for the formation of the little grains is rather small. For that reason, this process was not enough reproducible for large-scale production.

Nevertheless, the interest in the HPM material remained high and stimulated further research on the growth of Si ingots with small-sized grains.

A reproducible seeding procedure to achieve this kind of material is firstly reported by Lan et al. (2017). They used a layer of small Si chips or chunks, respectively, at the bottom of the crucible as seeds. This Si seeding layer is in fact a part of the Si feedstock material which makes the process step of the feedstock melting more difficult. The crucible heating must now be controlled – similar to the quasi-mono process (see Fig. 17 and section "Towards Monocrystals by Using Monocrystalline Seeds (Quasi-Mono QM)") – in order to leave an unmelted layer of the feedstock material.

In comparison to the *classic mc* and the *dendritic mc* described in section "Coarse Grain Structures Without Seed Crystals (Classic mc and Dendritic mc)," it is obvious that the mean grain size with typical values of ~1–4 mm^2 at the ingot bottom is quite smaller in the HPM material (compare Fig. 12a). In addition, the fraction of R-type grain boundaries is increased up to 70–75% in the HPM material whereas the number of twin grain boundaries is drastically decreased. This results in an even higher ratio of $R/\Sigma 3 > 3$ as sketched in Fig. 18. Finally, the HPM material exhibits quite lower dislocation content than *classic mc* Si material. All in all these structural properties of the HPM material are responsible for less areas of reduced minority carrier lifetime over the whole ingot volume and consequently also for higher cell efficiencies in comparison to classic mc Si wafers.

As a variety of feedstock materials are available on the market, one has to consider for the seeding layer several aspects. Firstly, the size and geometry of the particles have a strong influence to the penetration behavior of the Si melt into the seeding layer. Secondly, the particles and their microstructure have a direct influence on the grain structure which is growing on top of them. In a study of the authors group (Reimann et al. 2016), the use of various seeding feedstock materials like flat chips, edgy chunks, roundish granules or Si powder varying in size from µm to cm scale and also in microstructure (mono or multi) was investigated with respect to the resulting grain structure.

In cases where monocrystalline feedstock material (SCS) is used, the obtained mean grain size decreases with decreasing feedstock particle size, because each single feedstock particle acts as one monocrystalline seed, as shown in Fig. 32 on the left. Consequently the number of grains and also the number of grain boundaries increase the smaller the feedstock particles are. Further, the distribution of grain boundary types in such ingots is changed from a high ratio of twin/R (classic mc) to a high ratio of R/twin (HPM). In consequence, the relative length of R grain boundaries is quite higher than in the classic mc reference material. This is caused by the randomly distributed grain orientations which are predetermined by the feedstock particles. This is in contrast to the preferred grain orientations occurring during *classic mc* or *dendritic mc* growth (see section "Coarse Grain Structures Without Seed Crystals (Classic mc and Dendritic mc)"). Thereby, the smaller the grains and the more new grain boundaries are generated, the higher is the fraction of R grain boundaries. Reimann et al. (2016) have shown that it can increase up to 65% if feedstock particles are used with a size <1 mm.

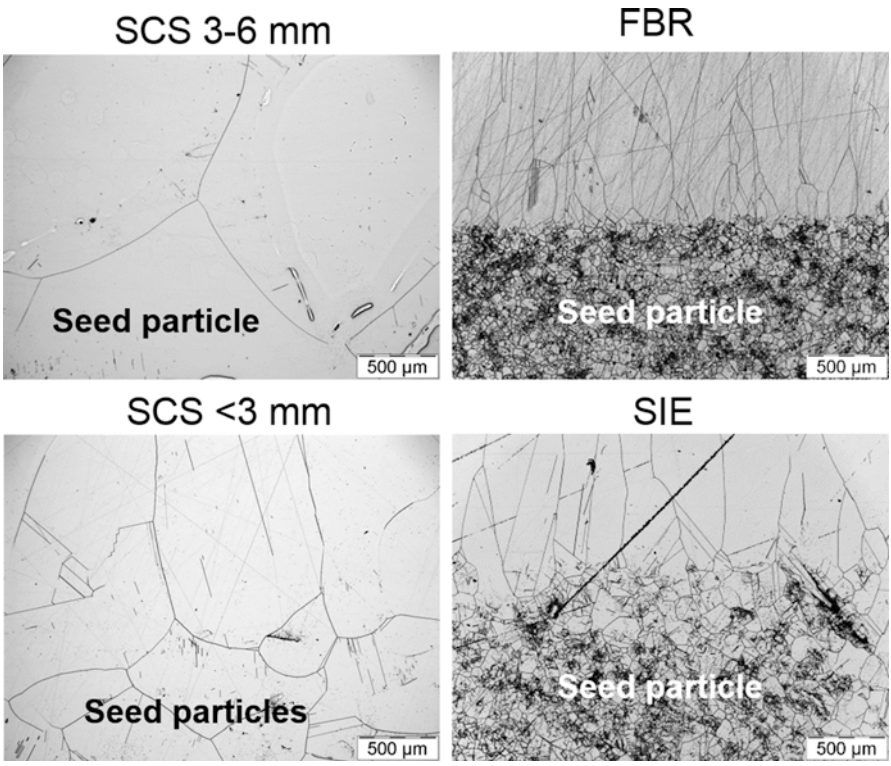

Fig. 32 Detailed images of vertical sections parallel to the direction of solidification with grain structures near the seeding position for: monocrystalline seed particles (left) and multicrystalline seeds (right). *SCS* single crystalline silicon, *FBR* fluidized Bed Reactor, *SIE* Siemens process. After Reimann et al. (2016)

Due to availability and purity issues, the more widespread approach is to use multicrystalline feedstock particles. The two main variants are Si chunks coming from the Siemens (SIE) process and roundish Si granules produced in a fluidized bed reactor (FBR). For those materials, the particle size does not influence the grain structure properties in that way as it is the case for the monocrystalline feedstock particles. The resulting R grain boundary fraction in the material seeded on SIE particles with a size between 0.2 and 15 mm as well as seeded on FBR granules with a size between 0.5 and 15 mm is on the same (constant) high level of 60–75% which is comparable to the value achieved with the monocrystalline particles with a size <1 mm. This can be related to the multicrystalline microstructure of the SIE and FBR material. According to their production processes, the feedstock particles exhibit internal grain sizes of 70–270 µm for Siemens and ~700 µm for FBR material (Ekstrøm et al. 2016b). All of these micrograins which come into contact with the Si melt act as nucleation centers and in consequence the mean size of the grains grown on top of the seed particles is in the same range as the dimensions of their microstructure (compare Fig. 32 on the right). However, the gaps between the

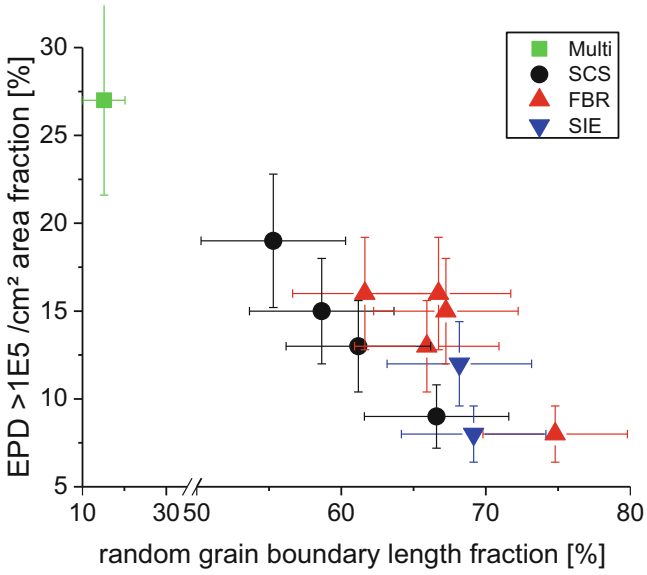

Fig. 33 Area fraction of wafer regions with etch pit densities EPD $> 10^5/cm^2$ versus the fractional amount of random (R) grain boundaries for wafers taken at 25 mm height from laboratory scale HPM Si ingots grown without seeds (multi), monocrystalline seeds (SCS) and multicrystalline seeds (SIE, FBR). After Reimann et al. (2016)

particles which were filled by Si melt are leading to relatively larger grains and therefore the resulting overall grain size is in the range of 1–3 mm^2.

As mentioned above, the high number of randomly oriented grains leads to a high fraction of R grain boundaries of more than 60% in the HPM material. These R-type grain boundaries are impeding the propagation of dislocations (see above). This property together with the small grain size are the main causes for the lower dislocation content and the significantly reduced wafer area covered by dislocation clusters in comparison to the classic mc Si material.

An experimental proof of this correlation is shown in Fig. 33 for laboratory-scale HPM Si ingots. The fractional amount of areas with dislocation clusters, i.e., an etch pit density (EPD) $> 10^5/cm^2$, is plotted versus the R grain boundary fraction. Obviously, the area fraction of highly dislocated regions can be suppressed below 10% if a high R grain boundary fraction around 70% is present in the HPM material.

Unfortunately, the positive effect of the R grain boundaries in HPM material diminishes more and more with increasing ingot height. It was found that the grain structure properties as well as the fractional amount of highly dislocated wafer area of *classical mc* and *HPM* wafers cut from the top regions of industrial ingots does not differ in such a way as it does in the bottom regions (Lehmann et al. 2016). Further, it was observed for industrial HPM ingots (e.g., by Lan et al. 2017) as well as for lab-scale HPM ingots (e.g., by Trempa et al. 2017) that the fraction of R grain

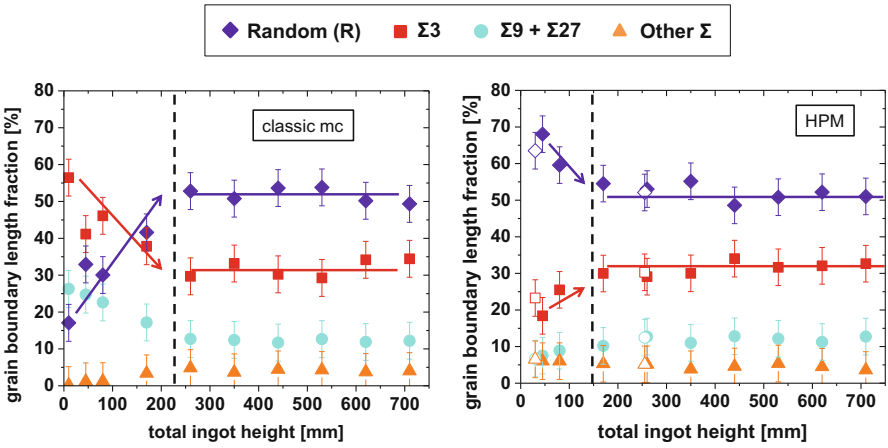

Fig. 34 Fraction of grain boundary length versus "total ingot height" (see text) for an ingot height of: classic mc G1 size (left) and G1 HPM ingot (right). Additionally, the values for a 300 mm industrial HPM ingot (open symbols) are shown in the right image. After Trempa et al. (2017)

boundaries drastically decreases within the first third of total ingot height. The reasons for this behavior are crystallographic grain boundary reactions which are thermodynamically driven to minimize the grain boundary energy. These processes are causing the annihilation of R grain boundaries, the generation of new twin boundaries and as a consequence a decrease of the R/Σ3 ratio with increasing ingot height (Prakash et al. 2015).

Trempa et al. (2017) simulated a DS process of a very large "total ingot height" of 710 mm by eight successive solidification steps with the same ingot (G1 size). The goal was to study the influence of the above mentioned grain boundary reactions in HPM material in comparison to conventional classic mc Si. The result is shown in Fig. 34 in terms of the fractional amount of the different types of grain boundaries versus the "total ingot height." Obviously, the grain boundary reactions take place in the firstly solidified 200 mm of the ingot height, irrespectively of the initially different distribution of grain boundary types in HPM and classic mc Si material. Above the height of about 200 mm, both types of materials (including the industrial ingot) reveal the same (constant) fractional amount of the different types of grain boundaries independently from the solidification process. This result holds also for the fraction of the highly dislocated wafer areas which become more and more equal and match each other at an ingot height of about 300–350 mm. This means that for ingot regions above 300 mm, there is no more benefit of the *HPM* material in comparison to the *classical mc* Si.

The main advantage of the "seeding on silicon" HPM growth method is the high reproducibility for the production of industrial ingots. In case that the seeding process is well controlled and suitable feedstock particles are used, the ingot manufacturer can be sure that the result will be a fine grained HPM material. However, there exist also some drawbacks of this method. First, the melting process

of the feedstock needs a more careful control in order to avoid the complete melting of the feedstock (seeding) layer and is more time consuming in comparison to the *classical mc* approach. A Si seed layer with a thickness of about 10–20 mm is necessary because of thermal process fluctuations. But it has to be mentioned that the remaining unmelted Si seed layer leads to an enlarged so-called "bottom red-zone" which results in an ingot part at the bottom region with a very low minority carrier lifetime value and consequently cannot be used for solar cell fabrication. Roughly spoken the length of the bottom red-zone of a HPM ingot is the sum of the red-zone length of a classic mc ingot plus the thickness of the seeding layer.

In summary, the yield losses of a HPM silicon ingot and a more expensive seeding procedure in comparison to a classic mc Si ingot are disadvantageous. To overcome these drawbacks, recent developments deal with seeding approaches without the use of a silicon feedstock layer, which will be the subject of the following section.

Fine Grain Structures Without Seeding on Si Material (HPM 2.0)

The common feature of all the new developed HPM seeding methods is to functionalize the crucible bottom in a way that the silicon feedstock can be completely melted as for the classical mc approach, but in contrast to classic mc a fine grained HPM structure is obtained. In principle, there exist three different approaches for the new processing, called "HPM 2.0," which can be used separately or in combination:

(a) Use of "foreign" (i.e., not Si) seed particles which are placed at the crucible bottom embedded or on top of the Si_3N_4 coating
(b) Modification of the surface of the Si_3N_4 coating concerning, e.g., morphology, wetting behavior, or roughness
(c) Modification of the structures of the crucible bottom by using certain contours like knobs or hillocks

For variant (a), it is important that the particles which support the nucleation have a higher melting point than silicon to avoid melting. Also they should exhibit a higher wettability as the surrounding Si_3N_4 coating in order to reduce the nucleation energy. But they must not contain harmful impurities like metals or dopants. Two materials which fulfill all the mentioned requirements are SiO_2 and SiC. Kupka et al. (2017) have tested them by spraying or embedding SiO_2/SiC particles with a size in the range of µm to mm on the bottom of G1 crucibles. The main conclusions of their results are the following:

- The mean grain size in the first grown part of the ingot decreases with increased surface roughness (Rq) of the nucleation layer and remains nearly constant at 1–2 mm^2 for Rq $>$ 200 µm

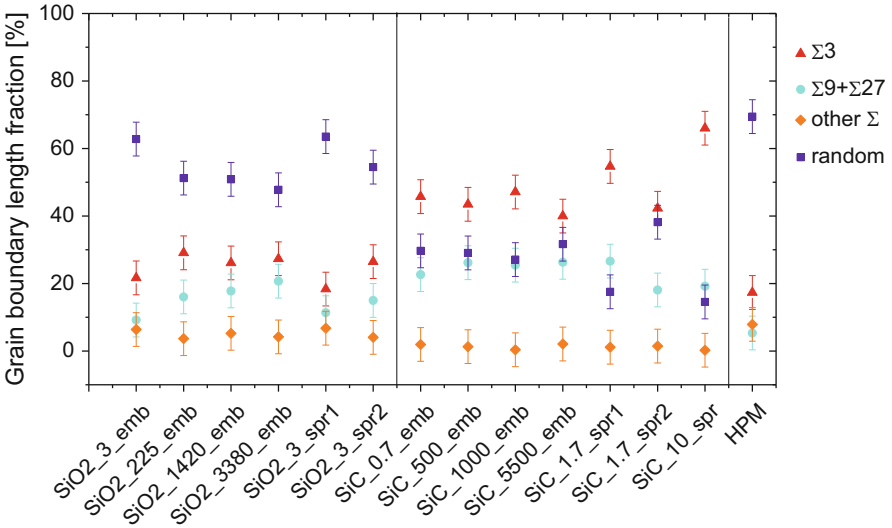

Fig. 35 Distribution of the grain boundary length fraction in dependence of the different used SiO_2 and SiC nucleation layers. After Kupka et al. (2017)

- Well wetted particles with a resulting mean grain size <4 mm^2 must not coercively lead to a high fraction of R grain boundaries over 50% (in the case of the SiC particles)
- Seed particles with low thermal conductivity are needed to achieve HPM properties (in the case of SiO_2 particles)

In summary, SiC particles are not suitable for generating a HPM grain structure with small grains *and* a high fraction of R grain boundaries. Even if relatively small grains grow, comparable to the SiO_2 seeding, the grain structure contains a high number of small dendrites and twins which is attributed to the high thermal conductivity of the SiC particles allowing higher supercoolings. In consequence, the resulting twin fraction is quite high and the R grain boundary fraction is always below 40% for all tested SiC nucleation layers (see Fig. 35 on the right), independently from the particle size (0.7–5000 μm) and the coating method (embedding or spraying).

In contrast to that, the SiO_2 particles with their low thermal conductivity could be identified as much promising seed material. In Fig. 35 on the left, it is shown that the fraction of R grain boundaries of all SiO_2 nucleation layers is significantly higher than of the SiC particles. In best cases, a R fraction of >60% is achievable if small (3 μm) particles are used.

Also on an industrial scale (G4 ingots), it was demonstrated, e.g., by Laurent et al. (2017) that the addition of small SiO_2 particles at the crucible bottom as functional seeds is a successful method to achieve a HPM grain structure. In Fig. 36, a result

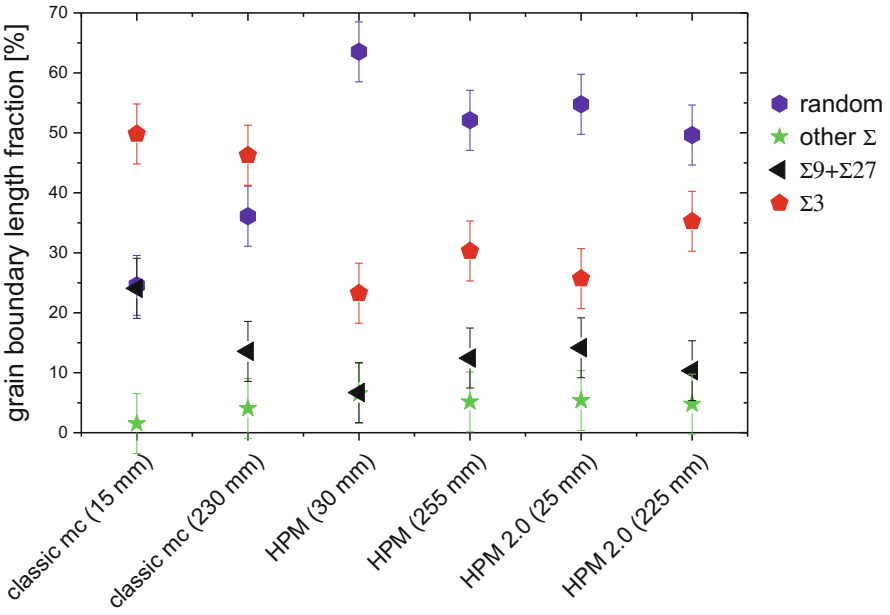

Fig. 36 Relative length of various types of grain boundaries in industrial scale G4 ingots for different process conditions: Standard (classic) mc-Si (left), reference HPM-mc Si (middle), and vesuvius HPM 2.0-mc Si (right). After Laurent et al. (2017)

with a relatively high fraction of R grain boundaries of 55–50% over ingot height is shown. This value is even better than that of the classical mc reference (25–35%) and only slightly below the conventional HPM values (65–55%) which were achieved by the Si self-seeding method. After making solar cells from these ingots, it could be demonstrated that the cell efficiency of the HPM 2.0 cells is ~0.5% absolutely higher than for the classic mc cells which matches the reported difference of conventional HPM versus classical mc in section "Fine Grain Structures with Seeding on Si Feedstock (Original HPM)."

The second approach (b) and the third approach (c) are not easy to separate and therefore it will be considered in the following as a "combination." For instance, Babu et al. (2016) presented a method where they positioned a monolayer of FBR Si feedstock granules at the bottom of a laboratory-scale crucible and coated it with a very thin layer of Si_3N_4. Due to the small thickness of the Si_3N_4 coating, the wavy morphology of the monolayer is maintained which is responsible for the nucleation behavior. A full melting process analogue to the classical mc approach was carried out up to 1470 °C for 1 h. However, it is not clear whether the FBR granules remained un-melted or whether they melted and resolidified by keeping their geometry due to the solid cover of Si_3N_4. The final results show that the fraction of R grain boundaries is at 55% close to the ingot bottom which is quite higher than

for the classical mc reference (18%). Also it was shown on etched wafers that the amount of dislocation clusters has significantly decreased.

A similar approach was shown by Zhang et al. (2016) who proposed a mask technique which allows to grow HPM 2.0 Si ingots in industrial G6 scale (840 × 840 mm). In this case a hillock structure of SiO_2 replaces the FBR granules used by Babu et al. (2016). Again the wavy structure was coated with a thin Si_3N_4 layer to prevent the adhesion of the Si ingot at the crucible/coating composite. In this case, the distribution of the grain boundary types was not investigated. However, the obtained results on solar cells imposingly show that the same cell efficiency distribution could be achieved over the whole G6 ingot with this method as for the conventional HPM approach using the seeding on mc silicon feedstock.

A further similar approach was proposed by Buchovska et al. (2017) who used an industrial G5 crucible containing silica knobs at its bottom to provide a "rough" nucleation layer. It is not mentioned whether these silica knobs were coated with Si_3N_4 or not. The grain boundary types were not investigated; however, results of PL measurements of a large series of wafers over the complete ingot reveal that the dislocation content is quite comparable to that one grown by a Si feedstock seeding method. Additionally, also cell efficiency data show comparable values for both material types.

In summary, one can state that the results obtained so far by using various approaches to replace the seeding on Si feedstock layer ("original" HPM) are promising. This holds for the achieved grain structures with respect to the dislocation problem and finally for the achieved cell efficiencies. However, it is not clear at that time which one of the different approaches has the potential to provide an increase of the material quality beyond the best HPM results.

Furthermore, it needs to be evaluated which of the different approaches can be implemented into production furnaces and is compatible with the routines of a production process.

Finally, it has to be demonstrated that certain reproducibility can be achieved for large ingot dimensions under production conditions. After that has been achieved, HPM2.0 can become an important DS production process which will then replace HPM and others.

Conclusions for Optimization Strategies with Respect to "Grain Boundary Engineering"

Actually, it is an open discussion, which Si material will dominate the PV market in the future. For 2017, the market share was around 20% classic mc, 40% HPM Si, and 40% mono CZ, whereas QM has not shown up in the statistics (ITRPV 2018). It seems to be sure that the high quality mono CZ material will play a significant role also in the future. The HPM Si will completely replace the classic mc in the near

future. However, whether the HPM Si will be also present after the next 5–10 years or if there is a comeback of the QM Si material is still open.

The possible cause is the tendency towards even higher solar cell efficiencies. All the modern solar cell concepts are based on monocrystalline silicon. Therefore, the gap between the efficiencies of mc-Si and mono Si solar cells might increase in the future, such that the cost per efficiency ratio for mono solar cells is superior to the mc-Si one. Therefore, it is forecasted that the share of mono Si wafers will increase in the future. Thus, wafer manufacturers have either to invest heavily in CZ pullers or to solve the existing challenges for QM silicon in order to run the industrial production of QM in the existing DS furnaces.

In fact, the HPM Si and the QM Si material need to be further developed to have a chance to be competitive with the CZ material. But for both growth technologies, the future progress depends on the control of the grain boundaries appearing in these materials.

In the case of the QM growth technology, the main task will be to reproducibly avoid the formation of dislocations and small angle grain boundaries induced by the seed joints. Here the grain boundary engineering with the most promising "SMART"-approach (see section "Towards Monocrystals by Using Monocrystalline Seeds (Quasi-Mono QM)") might be the best way to solve this problem even on an industrial scale. However, it is not clear whether sufficient good results could be reproducibly achieved by this method.

A perspective of the authors for improving the HPM material quality is to keep the fraction of random grain boundaries as high as possible along the complete ingot height. If this can be achieved the dislocation formation and movement is even more suppressed over longer growth heights and the amount of dislocation clusters should be further reduced. However, because the grain boundary formation and annihilation is also driven by a reduction of the grain boundary energy, it will be difficult to find practical solutions to overcome this physical law.

In general, for all DS growth technologies, the impurity contamination of the ingots will be an important issue in order to increase the Si material quality further. Higher purity of crucibles and Si_3N_4 coatings as well as cost-effective diffusion barriers between both components would be beneficial and would at the same time reduce the harmfulness of the grain boundaries in the Si due to a reduced impurity decoration.

Cross-References

- ▶ Defects in Crystalline Silicon: Dislocations
- ▶ Growth of Crystalline Silicon for Solar Cells: Czochralski Si
- ▶ Growth of Crystalline Silicon for Solar Cells: Mono-Like Method
- ▶ Growth of Multicrystalline Silicon for Solar Cells: Dendritic Cast Method
- ▶ Growth of Multicrystalline Silicon for Solar Cells: The High-Performance Casting Method
- ▶ Metal Impurities and Gettering in Crystalline Silicon
- ▶ Polysilicon and Its Characterization Methods

References

G.A. Babu, I. Takahashi, S. Matsushima, N. Usami, J. Cryst. Growth **441**, 124 (2016)

J. Bauer, O. Breitenstein, A. Lotnyk, H. Blumtritt, in *22nd European Photovoltaic Solar Energy Conference*, Milan (2007), p. 994

D.G. Brandon, Acta Metall. **14**, 1479 (1966)

I. Buchovska, O. Liaskovskiy, T. Vlasenko, S. Beringov, F.M. Kiessling, Sol. Energy Mater. Sol. Cells **159**, 128 (2017)

T. Buonassisi, M. Heuer, A.A. Istratov, M.D. Pickett, M.A. Marcus, B. Lai, Z. Cai, S.M. Heald, E.R. Weber, Acta Mater. **55**, 6119 (2007)

D. Camel, B. Marie, D. Ponthenier, F. Servant, in *3rd International Workshop on Crystalline Silicon Solar Cells,* Trondheim (2009)

J. Chen, T. Sekiguchi, D. Yang, Phys. Status Solidi C **4**, 2908 (2007)

M. Demant, S. Rein, J. Haunschild, T. Strauch, H. Höffler, J. Broisch, S. Wasmer, K. Sunder, O. Anspach, T. Brox, Prog. Photovolt. Res. Appl. **24**, 1533 (2016)

K.E. Ekstrøm, G. Stokkan, R. Søndenå, H. Dalaker, T. Lehmann, L. Arnberg, M. Di Sabatino, Phys. Status Solidi A **212**, 2278 (2015)

K.E. Ekstrøm, E. Undheim, G. Stokkan, L. Arnberg, M. Di Sabatino, Acta Mater. **109**, 267 (2016a)

K.E. Ekstrøm, G. Stokkan, A. Autruffe, R. Søndenå, H. Dalaker, L. Arnberg, M. Di Sabatino, J. Cryst. Growth **441**, 95 (2016b)

J. Friedrich, W. von Ammon, G. Müller, in *Handbook of Crystal Growth*, 2nd edn., ed. by P. Rudolph (Elsevier, Boston, 2015), p. 45

K. Fujiwara, W. Pan, N. Usami, K. Sawada, M. Tokairin, Y. Nose, A. Nomura, T. Shishido, K. Nakajima, Acta Mater. **54**, 3191 (2006)

D. Helmreich, in *Symposium on Electronic and Optical Properties of Polycrystalline or Impure Semiconductors and Novel Silicon Growth Methods,* St. Louis (Pennington, 1980), p. 184

D. Hu, S. Yuan, L. He, H. Chen, Y. Wan, X. Yu, D. Yang, Sol. Energy Mater. Sol. Cells **140**, 121 (2015)

Intego GmbH, Gemini-Grain structure analysis (2018), https://www.intego.de/de/solar1/pruefanlagen-fuer-die-solarfertigung/wafer/gemini-kornstrukturanalyse. Accessed 18 April 2018

ITRPV, *International Technology Roadmap for Photovoltaic (ITRPV) 2017* (2018)

M. Kohyama, R. Yamamoto, M. Doyama, Phys. Status Solidi B **138**, 387 (1986)

I. Kupka, T. Lehmann, M. Trempa, C. Kranert, C. Reimann, J. Friedrich, J. Cryst. Growth **465**, 18 (2017)

K. Kutsukake, N. Usami, Y. Ohno, Y. Tokumoto, I. Yonenaga, Appl. Phys. Express **6**, 25505 (2013)

K. Kutsukake, N. Usami, Y. Ohno, Y. Tokumoto, I. Yonenaga, IEEE J. Photovoltaics **4**, 84 (2014)

K. Kutsukake, M. Deura, Y. Ohno, I. Yonenaga, Jpn. J. Appl. Phys. **54**, 8 (2015)

C.W. Lan, W.C. Lan, T.F. Lee, A. Yu, Y.M. Yang, W.C. Hsu, B. Hsu, A. Yang, J. Cryst. Growth **360**, 68 (2012)

C.W. Lan, A. Lan, C.F. Yang, H.P. Hsu, M. Yang, A. Yu, B. Hsu, W.C. Hsu, A. Yang, J. Cryst. Growth **468**, 17 (2017)

J. Laurent, G. Rancoule, E. Drode, C. Reimann, M. Trempa, C. Kranert, J. Friedrich, L. Teale, R. Dyer, I. Dorrity, in *33rd European Photovoltaic Energy Specialist Conference,* Amsterdam (2017), p. 305

T. Lehmann, M. Trempa, E. Meissner, M. Zschorsch, C. Reimann, J. Friedrich, Acta Mater. **69**, 1 (2014)

T. Lehmann, C. Reimann, E. Meissner, J. Friedrich, Acta Mater. **106**, 98 (2016)

S. Martinuzzi, I. Périchaud, O. Palais, Sol. Energy Mater. Sol. Cells **91**, 1172 (2007)

K. Nakajima, K. Kutsukake, K. Fujiwara, N. Usami, S. Ono, Yamasaki, in *25th European Photovoltaic Solar Energy Conference,* Valencia (2010), p. 817

V. Oliveira, M. Tsoutsouva, T. Lafford, E. Pihan, F. Barou, C. Cayron, D. Camel, in *29th European Photovoltaic Solar Energy Conference,* Amsterdam (2014), p. 793

V. Oliveira, B. Marie, C. Cayron, M. Marinova, M.G. Tsoutsouva, H.C. Sio, T.A. Lafford, J. Baruchel, G. Audoit, A. Grenier, T.N. Tran Thi, D. Camel, Acta Mater. **121**, 24 (2016)

R.R. Prakash, K. Jiptner, J. Chen, Y. Miyamura, H. Harada, T. Sekiguchi, Appl. Phys. Express **8**, 35502 (2015)

V. Randle, *Microtexture Determination and its Applications*, 2nd edn. (Maney for the Institute of Materials Minerals and Mining, London, 2003)
C. Reimann, M. Trempa, T. Lehmann, K. Rosshirt, J. Stenzenberger, J. Friedrich, K. Hesse, E. Dornberger, J. Cryst. Growth **434**, 88 (2016)
B. Ryningen, G. Stokkan, M. Kivambe, T. Ervik, O. Lohne, Acta Mater. **59**, 7703 (2011)
D.G. Schimmel, J. Electrochem. Soc. **126**, 479 (1979)
F. Schmid, U.S. Patent 3,898,051, 1975
F. Secco D'Aragona, Solid State Sci. Technol. **119**, 948 (1972)
E. Sirtl, A. Adler, Z. Metallkd./Mater. Res. Adv. Tech. **52**, 529 (1961)
B.L. Sopori, J. Electrochem. Soc. **131**, 667 (1984)
B. Sopori, D. Guhabiswas, P. Rupnowski, S. Shet, S. Devayajanam, H. Moutinho, in *36th IEEE Photovoltaic Specialists Conference,* Seattle (2011), p. 1680
N. Stoddard, Patent WO 2009/014957 A2, 29 Jan 2009
N. Stoddard, W. Bei, I. Witting, M. Wagener, P. Yongkook, G. Rozgonyi, R. Clark, Solid State Phenom. **131–133**, 1 (2008)
I. Takahashi, S. Joonwichien, T. Iwata, N. Usami, Appl. Phys. Express **8**, 105501 (2015)
M. Trempa, *Gerichtete Erstarrung von einkristallinen Siliciumkristallen nach dem VGF-Verfahren für die Anwendung in der Photovoltaik* (Fraunhofer-Verlag, Stuttgart, 2014)
M. Trempa, C. Reimann, J. Friedrich, G. Müller, D. Oriwol, J. Cryst. Growth **351**, 131 (2012)
M. Trempa, C. Reimann, J. Friedrich, G. Müller, A. Krause, L. Sylla, T. Richter, J. Cryst. Growth **405**, 131 (2014)
M. Trempa, C. Reimann, J. Friedrich, G. Müller, L. Sylla, A. Krause, T. Richter, J. Cryst. Growth **429**, 56 (2015a)
M. Trempa, C. Reimann, J. Friedrich, G. Müller, A. Krause, L. Sylla, T. Richter, Cryst. Res. Technol. **50**, 124 (2015b)
M. Trempa, M. Beier, C. Reimann, K. Roßhirth, J. Friedrich, C. Löbel, L. Sylla, T. Richter, J. Cryst. Growth **454**, 6 (2016)
M. Trempa, I. Kupka, C. Kranert, T. Lehmann, C. Reimann, J. Friedrich, J. Cryst. Growth **459**, 67 (2017)
S. Tsurekawa, K. Kido, T. Watanabe, Mater. Sci. Eng. A **462**, 61 (2007)
D.S. Vlachavas, Acta Crystallogr. A **41**, 530 (1985)
F. Wilhelm, J. Appl. Crystallogr. **4**, 521 (1971)
M. Wright-Jenkins, J. Electrochem. Soc. **124**, 757 (1977)
K.H. Yang, J. Electrochem. Soc. **131**, 1140 (1984)
Y.M. Yang, A. Yu, B. Hsu, W.C. Hsu, A. Yang, C.W. Lan, Prog. Photovolt. Res. Appl. **23**, 340 (2015)
H. Zhang, D. You, C. Huang, Y. Wu, Y. Xu, P. Wu, J. Cryst. Growth **435**, 91 (2016)